

Kondo scattering in underdoped $\text{Nd}_{1-x}\text{Sr}_x\text{NiO}_2$ infinite-layer superconducting thin films

T. N. Shao¹, Z. T. Zhang¹, Y. J. Qiao¹, Q. Zhao¹, H. W. Liu^{1*}, X. X. Chen¹, W. M. Jiang¹, C. L. Yao¹, X. Y. Chen¹, M. H. Chen¹, R. F. Dou¹, C. M. Xiong¹, G. M. Zhang^{2,3*}, Y.-F. Yang^{4,5,6*}, J. C. Nie^{1*}

¹*Department of Physics, Beijing Normal University, Beijing 100875, China*

²*State Key Laboratory of Low-Dimensional Quantum Physics and Department of Physics, Tsinghua University, Beijing 100084, China*

³*Frontier Science Center for Quantum Information, Beijing 100084, China*

⁴*Beijing National Laboratory for Condensed Matter Physics and Institute of Physics, Chinese Academy of Sciences, Beijing 100190, China*

⁵*School of Physical Sciences, University of Chinese Academy of Sciences, Beijing 100190, China*

⁶*Songshan Lake Materials Laboratory, Dongguan, Guangdong 523808, China*

*Corresponding author. E-mail: jcnie@bnu.edu.cn (J.C.N.); yifeng@iphy.ac.cn (Y.-F.Y.); gmzhang@tsinghua.edu.cn (G.M.Z.); haiwen.liu@bnu.edu.cn (H.W.L.)

The recent discovery of superconductivity in infinite-layer nickelates generates tremendous research endeavors, but the ground state of their parent compounds is still under debate. Here, we report experimental evidences for the dominant role of Kondo scattering in the underdoped $\text{Nd}_{1-x}\text{Sr}_x\text{NiO}_2$ thin films. A resistivity minimum associated with logarithmic temperature dependence in both longitudinal and Hall resistivities are observed in the underdoped $\text{Nd}_{1-x}\text{Sr}_x\text{NiO}_2$ samples before the superconducting transition. A linear scaling behavior $\sigma_{xy}^{\text{AHE}} \sim \sigma_{xx}$ between anomalous Hall conductivity σ_{xy}^{AHE} and conductivity σ_{xx} is revealed, verifying the dominant Kondo scattering at low temperature. The effect of weak (anti-)localization is found to be secondary. Our experiments can help clarifying the basic physics in the underdoped $\text{Nd}_{1-x}\text{Sr}_x\text{NiO}_2$ infinite-layer thin films.

The mechanism of high- T_c superconductivity remains a long-standing mystery, even though tremendous efforts and significant advances have been made in the study of cuprates and Fe-based superconductors. Aiming to mimic the cuprate-like electronic configuration, superconductivity has been proposed and recently found in the infinite-layer nickelate compounds [1]. This discovery has drawn enormous attention [2-6] since it may provide deeper insight about the pairing mechanism of unconventional superconductivity. But instead of an antiferromagnetic (AFM) order in the cuprates, the parent compound of superconducting nickelates shows no sign of static long-range magnetic order down to 1.7 K by neutron diffraction [7] and down to 2 K by muon spin measurements [8] in bulks and also a lack of long-range AFM in thin films [9], despite their

similarities in the crystalline and electronic structures with the formal $3d^9$ configuration. Moreover, unlike the cuprates where doped holes reside on the oxygen atoms, here they are mainly introduced into Ni $3d$ states and reside in the $3d_{x^2-y^2}$ orbitals [10], supported by the softening of resonant inelastic x-ray scattering (RIXS) [11]. Besides, superconductivity remains absent in infinite-layer nickelate bulk, although the application of pressure up to 50.2 GPa can significantly suppress the insulating behavior [12,13]. This raises a question regarding whether the cuprates and hole doped NdNiO_2 share the same mechanism of superconductivity [14]. In the experimental aspect, controlling the doping concentration and studying its relationship with T_c has become a necessary step to understand the electron interaction in nickelate systems. A non-monotonic relationship between T_c and Sr doping concentration is established [3,15], reminiscent of the competition between superconductivity and adjacent phase (or its phase fluctuation) in unconventional superconductors [16-18]. It is therefore important to understand the underdoped nickelates, where, different from the cuprates, the resistivity shows metallicity at high temperatures and weak insulating behavior at low temperatures.

In order to explain the resistivity upturn at low temperatures, Zhang et al. [19] proposed a self-doped Mott-Kondo scenario for the parent nickelate system, bridging the Kondo lattice model for heavy fermions and the t-J model for cuprates. It was proposed that self-doping, namely charge transfer from localized Ni $3d$ orbitals to other conduction bands, plays an essential role. The remaining Ni $3d$ local moments may couple to the conduction electrons, causing the well-known Kondo screening physics [20] and giving rise to Kondo scattering that explains the low temperature resistivity upturn reported in NdNiO_2 [1], LaNiO_2 [9], as well as underdoped infinite-layer $\text{Nd}_{1-x}\text{Sr}_x\text{NiO}_2$ ($x = 0.1, 0.125$) [15]. The absence of long-range magnetic ordering [9] might also be attributed to the self-doping and the Kondo screening effect. However, in addition to other theoretical scenarios including the pseudogap [21], magnetic scattering [22] and the d-wave order [23], the logarithmic temperature dependence of resistivity at low temperatures has also been observed in underdoped cuprates and was mainly attributed to the weak localization (WL) [24-26]. Although it has been argued theoretically [5,27] that the transport properties of the underdoped nickelates are very different from that of the AFM cuprate Mott insulator, whether the $\ln T$ behavior in the underdoped nickelates is caused by the Kondo effect or by the WL effect has not been determined, which leads to unsettled debate concerning the basic physics of the nickelate superconductors. The transport measurements including both

longitudinal and transverse resistivity are therefore indispensable to uncover the low-energy excitations of the parent compounds of nickelate superconductor and provide decisive evidence for different theoretical proposals to understand the unconventional superconductivity in nickelate system.

Here, we study the normal-state transport properties of the infinite-layer $\text{Nd}_{1-x}\text{Sr}_x\text{NiO}_2$ thin films with a low Sr doping concentration. Our preliminary analysis of the film reveals a $\ln T$ behavior in both resistivity and R_H in the same temperature region. A linear dependence of the anomalous Hall-effect (AHE) conductance $\sigma_{xy}^{AHE} \sim \sigma_{xx}$ indicates that the skew scattering is dominant in the exact same temperature range. The dephasing rate shows a linear temperature dependence at temperatures below T_K , in good agreement with the Kondo scenario. The WL contribution is shown to be secondary. Our experimental results strongly support the self-doped Mott-Kondo scenario for the underdoped $\text{Nd}_{1-x}\text{Sr}_x\text{NiO}_2$ infinite-layer superconducting thin films.

$\ln T$ resistance. — Figure 1a shows the temperature-dependent resistivity $\rho(T)$ for the underdoped $\text{Nd}_{0.88}\text{Sr}_{0.12}\text{NiO}_2$ thin film. A superconducting transition is observed, with an onset at 4.06 K and a midpoint at 0.79 K. The broad transition indicates the inhomogeneity of the infinite-layer thin film. These observations reveal that the infinite-layer nickelate phase (the structural characterizations are shown in Supplementary Figs. 1-2), not the reduced secondary phase, is superconducting. As shown in Fig. 1a, the resistivity of the $\text{Nd}_{0.88}\text{Sr}_{0.12}\text{NiO}_2$ thin film first decreases as the temperature decreases, followed by a resistivity minimum at a characteristic temperature $T^* \sim 40$ K. The minimum resistivity (~ 0.80 m Ω ·cm at 40 K) falls below the value of 0.87 m Ω ·cm that corresponds to the quantum sheet resistance ($h/e^2 \sim 26$ k Ω) per NiO_2 two-dimensional plane, which is consistent with the previous report [15]. Below 30 K down to 7 K, the resistivity shows logarithmic temperature dependence regardless of the magnetic field (see Fig. 1b). In fact, this characteristic is commonly observed in all our underdoped $\text{Nd}_{1-x}\text{Sr}_x\text{NiO}_2$ infinite-layer thin films, as shown in Fig. 1c. We find that the ρ - T curves can be well described by Hamann model from 8 K to 120 K [28],

$$\rho(T) = \rho_0 + aT^2 + bT^5 + \rho_K(T/T_K) \quad (1)$$

where ρ_0 is the residual resistivity caused by sample disorder and the T^2 and T^5 terms are the contributions of electron-electron and phonon-electron interactions, respectively. $\rho_K(T/T_K)$ is the resistivity induced by magnetic scattering in the absence of magnetic field [28-30] and takes the form,

$$\rho_K(T/T_K) = \frac{2\pi c\hbar}{ne^2k_F} \left\{ 1 - \ln(T/T_K) \cdot [\ln^2(T/T_K) + s(s+1)\pi^2]^{-1/2} \right\} \quad (2)$$

where $k_F = 2\pi \left(\frac{3n}{8\pi}\right)^{1/3}$ is the Fermi wave-vector in a free electron approximation. The best fitting results to the ρ - T curves of underdoped $\text{Nd}_{1-x}\text{Sr}_x\text{NiO}_2$ samples using Eqs. (1) and (2) are shown in Supplementary Fig. 5. Moreover, we have carried out low-temperature transport measurements in magnetic field for three underdoped $\text{Nd}_{1-x}\text{Sr}_x\text{NiO}_2$ samples ($x = 0, 0.05, 0.09$). All three underdoped samples are well consistent with the Kondo scattering scenario [20] down to 0.04 K. The numerical renormalization group (NRG) fitting, non-crossing approximation (NCA) fitting (see Fig. 1d and Supplementary Fig. 4) and Hamann fitting (Supplementary Fig. 5) curves provide quantitative justification for this point. The magnetic field truly influences the R - T curves of underdoped samples with pronounced negative magnetoresistance (as shown in Supplementary Fig. 5), reminiscent of the well-known negative magnetoresistance in Kondo system (La, Ce)Al₂ [31]. Moreover, all the underdoped samples (Fig. 1d) demonstrate clear feature of Kondo scattering in temperature regime above T_K . The good agreement with the NRG, NCA, and Hamann predictions proves exclusively the Kondo mechanism and leaves little room for other interpretation in underdoped region, which also confirms that the local moment is roughly spin-1/2. This excludes its possible origin from the Nd 4f spin ($S=3/2$) and supports its origin from the Ni $3d_{x^2-y^2}$ moment.

Pinpoint the Kondo scattering mechanism.—Remarkably, for temperatures below 40 K down to 6 K, the R_H follows closely that of the resistivity ρ , and resembles the $\ln T$ dependence of the resistivity, as shown in Fig. 2a. The $R_H \propto \rho$ behavior is well consistent with the theoretical prediction of Kondo skew scattering associated with local moments [32,33]. Thus, both the resistivity and Hall coefficient support the presence of the magnetic Kondo scattering in the underdoped nickelate superconductor. The relation between σ_{xy}^{AHE} and σ_{xx} can further confirm the skew scattering mechanism characterized by $\sigma_{xy}^{\text{AHE}} \propto \sigma_{xx}$ in a temperature range of 7–40 K for the $\text{Nd}_{0.88}\text{Sr}_{0.12}\text{NiO}_2$ thin film (see Fig. 2b). The conductivity σ_{xx} of the $\text{Nd}_{0.88}\text{Sr}_{0.12}\text{NiO}_2$ is about $10^3 \Omega^{-1}\text{cm}^{-1}$ and is in a bad metal regime [33], in which σ_{xy}^{AHE} should generally decrease with decreasing σ_{xx} at a rate faster than linear. Nevertheless, by subtracting the ordinary Hall effect (OHE) contribution (R_0 , which is determined by the measured Hall coefficients and the Curie-Weiss fit and does not change with varying temperature, see detailed discussion in Eqs. (4) and (5) and results in Fig. 3a) to obtain σ_{xy}^{AHE} from σ_{xy} , a linear dependence of $\sigma_{xy}^{\text{AHE}} \propto \sigma_{xx}$ is observed in the temperature range of

7–40 K. This temperature range is the same as the range where resistivity shows logarithmic temperature dependence (see Fig. 2a). These observations strongly support that the incoherent skew scattering [32,33] is a dominant mechanism for understanding our $R_H(T)$ results. At high temperatures (> 40 K), the Kondo scattering is suppressed and a deviation from the linear dependence between σ_{xy}^{AHE} and σ_{xx} is also observed.

One may argue that the logarithmic temperature dependence of resistivity at low temperatures, a hallmark of the Kondo effect, could also originate from the weak localization/weak anti-localization (WL/WAL) in two-dimensional system. However, as shown in Fig. 1c, the $\ln T$ correction of resistivity under large magnetic field can exclude the WL/WAL correction and justify the Kondo scattering scenario. The conductance correction due to the Kondo effect can be obtained with $\Delta\sigma_{\text{Kondo}} = \sigma(T) - \sigma(T_{\text{min}} = 40\text{K})$ (zero field) and the data (extracted from Fig. 1b) are shown in Fig. 3a. The red line is the $e^2/\pi h \cdot \ln T$ fit for $\Delta\sigma$, the obtained slope is $\beta \approx 6.96$ for the temperature range of 8–24 K. Although both the WL/WAL and the electron-electron interaction (EEI) in two-dimensional system also contribute to a conductance correction proportional to $e^2/\pi h \cdot \ln T$, the total value for the coefficient of WL/WAL and EEI corrections is commonly less than 2 [34]. Thus, the value of β is much larger than the typical value contributed from WL/WAL and EEI effect (see the Supplementary Note 1) [30]. In order to single out the WL/WAL correction, the measurement in a modest magnetic field (*e.g.*, $H = 4$ T) is necessary (Supplementary Fig. 8) [30]. The conduction correction due to the WL/WAL effect can be obtained with $\Delta\sigma_{\text{WL/WAL}} = \sigma(T)|_{H=0} - \sigma(T)|_{H=4\text{T}}$, and the data are shown in the inset of Fig. 2c. The blue line is the $\ln T$ fit, the obtained slope is $\Delta\kappa = \alpha p \approx 0.213$ (p is the dephasing exponent, $\tau_\phi^{-1} \sim T^p$) for the temperature range of 10–20 K, much less than the total value $\beta \approx 6.96$, indicating that the WL/WAL is a secondary effect and Kondo scattering is dominant in the temperature range of 7–30 K.

Moreover, we can also utilize the low field magneto-conductivity to analyze the temperature dependence of electron dephasing, based on the modified Hikami-Larkin-Nagaoka (HLN) formula [35]:

$$\Delta\sigma(H) = \frac{\alpha e^2}{\pi h} \left[\Psi \left(\frac{1}{2} + \frac{H_\phi}{H} \right) - \ln \frac{H_\phi}{H} \right], \quad (3)$$

where Ψ is the digamma function, $H_\phi = \hbar/4eD\tau_\phi$, D is the electronic diffusion constant, and α is an effective constant depending on the relative strengths of magnetic scattering and spin-orbit coupling (See

Supplementary Figs. 8-9 for related results and see Supplementary Figs. 10-15 for detailed analysis) [30]. As shown in the inset of Fig. 2d, for the nickelate thin film studied in this work, a small positive value $\alpha \approx 0.20$ can be maintained for a wide temperature range of 9–20 K. As the dephasing rate τ_φ^{-1} is simply proportional to H_φ , there exists a linear power-law dependence: $H_\varphi \sim T^p$ with $p \approx 1$. Indeed, as shown in Fig. 2d, a linear temperature dependence of the dephasing field H_φ is observed over a wide temperature range of 8–16 K below T_K , which is consistent with the universal dephasing rate due to diluted Kondo impurities [36]. The dephasing field H_φ exhibits a deviation from the linearity around ~ 16.0 K. This is another definition of T_K [37,38], and the obtained value (16.0 K) is well consistent with that (~ 15.6 K, see Supplementary Fig.5d) determined by the resistivity measurements. Thus, the Kondo scenario provides a consistent explanation of all our measured data.

Phase diagram.—Figure 3a displays the Hall-effect measurements obtained in large temperature range under an applied field of 9 T, showing negative Hall coefficients (R_H) with a maximum at $T^* \sim 40$ K. Interestingly, we find the Hall coefficients now follow a simple Curie-Weiss law. To see this, we separate the normal coefficient R_0 from the AHE coefficient and make the ansatz based on the treatment of heavy fermion superconductors [39]

$$\rho_{xy} = R_0 H + 4\pi M R_S. \quad (4)$$

Taking $M = \chi H$, $\chi = C/(T - \Theta)$, we have

$$R_H = \frac{\rho_{xy}}{H} = R_0 + 4\pi \frac{C}{T - \Theta} R_S = R_0 + \frac{R_S'}{T - \Theta}, \quad (5)$$

with three fitting parameters. R_0 is the OHE coefficient due to the deflection of the conduction electrons by the Lorentz force. We obtain a good fit which satisfies the Curie-Weiss law for $60 \text{ K} \leq T \leq 300 \text{ K}$. The best fit (solid line in Fig. 3a) was obtained at $R_0 = -2.61 \times 10^{-3} \text{ cm}^3 \text{ C}^{-1}$, $\Theta = -66.45 \text{ K}$ and $R_S' = 0.20 \text{ cm}^3 \text{ K C}^{-1}$. R_0 was found to be negative, which means that the OHE is dominated by electrons. This is consistent with the band structure calculations revealing that the parent NdNiO_2 contains small electron pockets at the Fermi energy [40]. The fitting value R_0 corresponds to 0.12 electron per formula unit. As shown in Fig. 3b, the Hall resistivity ρ_{xy} versus magnetic field up to 35 T at temperatures from 10 K to 70 K shows no obvious deviation from linear dependence on magnetic field (also see Supplementary Fig. 7 for the extended temperature region data). Such Curie-Weiss type temperature dependence of the positive AHE coefficient is repeatedly

observed in our underdoped $\text{Nd}_{1-x}\text{Sr}_x\text{NiO}_2$ infinite-layer thin films (as shown in Fig. 3c) and is also common in recently reported nickelate superconductors [3,14,15,41]. It supports the existence of free local moments at high temperatures where the Kondo scattering is negligible and the resistivity is dominated by electron-phonon scattering. The negative values of the Weiss temperature Θ indicate AFM correlations in the localized-spin systems. Actually, a magnetic ground state is often obtained in theoretical studies [6,10,40,42,43]. A branch dispersion of magnetic excitations in undoped NdNiO_2 has recently been revealed using RIXS [44], suggesting a spin wave of strongly coupled, antiferromagnetically aligned spins on a square lattice. A recent NMR study shows the presence of AFM fluctuations and quasi-static AFM order in $\text{Nd}_{0.85}\text{Sr}_{0.15}\text{NiO}_2$ [45] thin film. However, the tendency towards a long-range AFM order is interrupted by the self-doping and Kondo screening effect, causing a paramagnetic state (Fig. 2a and Supplementary Fig. 6) [30] as reported so far for all RNiO_2 (R = rare-earth) parent materials [7,9].

Based on the present findings, Fig. 3d depicts a phase diagram of the $\text{Nd}_{1-x}\text{Sr}_x\text{NiO}_2$ showing a superconducting dome, combined with that in recent reports [3,15,46,47], and the characteristic temperature T^* , where the R_H shows a maximum. As x increases from the underdoped side, T^* decreases monotonically and the T^*-x curve separates the underdoped region into two parts: a Kondo scattering region and a metal. It is worth noting that the extension of the T^*-x curve reaches the bottom of the superconducting dome (under field). Thus, instead of a simple Mott insulator, the Kondo physics must also play a crucial role in nickelate superconductors. Our results may indeed have some implications on the superconductivity. Based on the Kondo mechanism in the underdoped region, our phase diagram (see Fig. 3d) suggests that superconductivity emerges near the boundary that the Kondo effect is suppressed. As discussed previously [19], this may have important influence on the pairing symmetry of the superconductivity. The interplay of magnetic fluctuations and Kondo hybridization could potentially lead to $d + is$ pairing [19].

Putting together, the logarithmic temperature dependence of resistivity and R_H , the good agreement with the NRG, NCA, and Hamann predictions, the linear dependence of $\sigma_{xy}^{\text{AHE}} \sim \sigma_{xx}$, and the linear temperature dependence of the dephasing rate, all support the presence of the magnetic Kondo scattering in the underdoped infinite-layer $\text{Nd}_{1-x}\text{Sr}_x\text{NiO}_2$ thin film. According to Zhang et al. [19], the presence of local

moments cannot be ascribed to the Nd 4f moments since similar transport properties have also been observed in LaNiO₂ [9]. The first-principles band structure calculations [40] show that the Nd 5d orbitals in NdNiO₂ are hybridized with the Ni 3d orbitals, leading to small Fermi pockets of dominantly Nd 5d electrons in the Brillouin zone. Nd 5d conduction electrons have an electron density of $n < 1$ per Ni site, coupled to the localized Ni¹⁺ spin-1/2 of $3d_{x^2-y^2}$ orbital to form Kondo spin singlets, as in the Kondo lattice systems with a small concentration of conduction electrons [20]. The fitted magnetic impurity concentration (~ 0.03 per formula unit, see Supplementary Fig.5d) is comparable with that of dilute Kondo systems [39]. In conclusion, our experimental results strongly support the self-doped Mott-Kondo scenario for the underdoped Nd_{1-x}Sr_xNiO₂ infinite-layer thin films. The present findings shed new light on the underlying physics of the infinite-layer nickelates and a possibly novel mechanism of unconventional superconductivity. It would improve our understanding of the newly discovered superconductivity in nickelates.

This work was supported by the National Natural Science Foundation of China (Grants No. 92065110, No. 11974048, No. 12074334, No. 12174429, No. 12022407), the National Basic Research Program of China (Grants No. 2014CB920903 and No. 2013CB921701), and the Strategic Priority Research Program of the Chinese Academy of Sciences (Grant No. XDB33010100) for their financial support. This work was also supported by the High Magnetic Field Laboratory of Chinese Academy of Sciences at Hefei.

References

- [1] D. Li, K. Lee, B. Y. Wang, M. Osada, S. Crossley, H. R. Lee, Y. Cui, Y. Hikita, and H. Y. Hwang, Superconductivity in an infinite-layer nickelate, *Nature* **572**, 624-627 (2019).
- [2] Q. Gu, Y. Li, S. Wan, H. Li, W. Guo, H. Yang, Q. Li, X. Zhu, X. Pan, Y. Nie, and H.-H. Wen, Single particle tunneling spectrum of superconducting NiNd_{1-x}Sr_xNiO₂ thin films, *Nat. Commun.* **11**, 6027 (2020).
- [3] S. Zeng, C. S. Tang, X. Yin, C. Li, M. Li, Z. Huang, J. Hu, W. Liu, G. J. Omar, H. Jani, Z. S. Lim, K. Han, D. Wan, P. Yang, S. J. Pennycook, Andrew T. S. Wee, and A. Ariando, Phase diagram and superconducting dome of infinite-layer Nd_{1-x}Sr_xNiO₂ thin films, *Phys. Rev. Lett.* **125**, 147003 (2020).
- [4] B. H. Goodge, D. Li, K. Lee, M. Osada, B. Y. Wang, G. A. Sawatzky, H. Y. Hwang, and L. F. Kourkoutis, Doping evolution of the Mott–Hubbard landscape in infinite-layer nickelates, *Proc. Nat. Acad. Sci.* **118**, e2007683118 (2021).
- [5] Y.-H. Zhang, and A. Vishwanath, Type-II t–J model in superconducting nickelate Nd_{1-x}Sr_xNiO₂, *Phys. Rev. Res.* **2**, 023112 (2020).
- [6] A. S. Botana, and M. R. Norman, Similarities and Differences between LaNiO₂ and CaCuO₂ and Implications for Superconductivity, *Phys. Rev. X* **10**, 011024 (2020).
- [7] M. A. Hayward, and M. J. Rosseinsky, Synthesis of the infinite layer Ni(I) phase NdNiO_{2+x} by low

- temperature reduction of NdNiO₃ with sodium hydride, *Solid State Sci.* **5**, 839-850 (2003).
- [8] R. A. Ortiz, P. Puphal, M. Klett, F. Hotz, R. K. Kremer, H. Trepka, M. Hemmida, H.-A. Krug von Nidda, M. Isobe, R. Khasanov, H. Luetkens, P. Hansmann, B. Keimer, T. Schäfer, and M. Hepting, Magnetic correlations in infinite-layer nickelates: An experimental and theoretical multimethod study, *Phys. Rev. Research* **4**, 023093 (2022).
- [9] A. Ikeda, Y. Krockenberger, H. Irie, M. Naito, and H. Yamamoto, Direct observation of infinite NiO₂ planes in LaNiO₂ films, *Appl. Phys. Express* **9**, 061101 (2016).
- [10] H. Zhang, L. Jin, S. Wang, B. Xi, X. Shi, F. Ye, and J.-W. Mei, Effective Hamiltonian for nickelate oxides Nd_{1-x}Sr_xNiO₂, *Phys. Rev. Res.* **2**, 013214 (2020).
- [11] M. Rossi, H. Lu, A. Nag, D. Li, M. Osada, K. Lee, B. Y. Wang, S. Agrestini, M. Garcia-Fernandez, J. J. Kas, Y.-D. Chuang, Z. X. Shen, H. Y. Hwang, B. Moritz, Ke-Jin Zhou, T. P. Devereaux, and W. S. Lee, Orbital and spin character of doped carriers in infinite-layer nickelates, *Phys. Rev. B* **104**, L220505 (2021).
- [12] Q. Li, C. He, J. Si, X. Zhu, Y. Zhang, and H.-H. Wen, *Absence of Superconductivity in Bulk Nd_{1-x}Sr_xNiO₂*, *Comms. Mater.* **1**, 16 (2020).
- [13] Q. Gu, and H.-H. Wen, *Superconductivity in Nickel-Based 112 Systems*, *The Innovation* **3**, 100202 (2022).
- [14] Y. Ji, J. Liu, L. Li, and Z. Liao, Superconductivity in infinite layer nickelates, *J. Appl. Phys.* **130**, 060901 (2021).
- [15] D. Li, B. Y. Wang, K. Lee, S. P. Harvey, M. Osada, B. H. Goodge, L. F. Kourkoutis, and H. Y. Hwang, Superconducting Dome in Nd_{1-x}Sr_xNiO₂. Infinite Layer Films, *Phys. Rev. Lett.* **125**, 027001 (2020).
- [16] B. Keimer, S. A. Kivelson, M. R. Norman, S. Uchida, and J. Zaanen, From quantum matter to high-temperature superconductivity in copper oxides, *Nature* **518**, 179-186 (2015).
- [17] Hosono, H. Layered Iron Pnictide Superconductors: discovery and current status, *J. Phys. Soc. Jpn.* **77**, 1-8 (2008).
- [18] E. Dagotto, Complexity in Strongly Correlated Electronic Systems, *Science* **309**, 257-262 (2005).
- [19] G.-M. Zhang, Y.-F. Yang, and F.-C. Zhang, Self-doped Mott insulator for parent compounds of nickelate superconduct, *Phys. Rev. B* **101**, 020501(R) (2020); Y.-F. Yang, and G.-M. Zhang, Self-doping and the Mott-Kondo scenario for infinite-layer nickelate superconductors, *Front. Phys.* **9**, 801236 (2022).
- [20] A. C. Hewson, *The Kondo Problem to Heavy Fermions* (Cambridge University Press, Cambridge, UK, 1993); T. A. Costi, A. C. Hewson, and V. Zlatic, *J. Phys.: Condens. Matter* **6**, 2519 (1994).
- [21] F. Laliberté, W. Tabis, S. Badoux, B. Vignolle, D. Destraz, N. Momono, T. Kurosawa, K. Yamada, H. Takagi, N. Doiron-Leyraud, C. Proust, and Louis Taillefer, Origin of the metal-to-insulator crossover in cuprate superconductors, arXiv:1606.04491.
- [22] Y. Dagan, M. C. Barr, W. M. Fisher, R. Beck, T. Dhakal, A. Biswas, and R. L. Greene, Origin of the Anomalous Low Temperature Upturn in the Resistivity of the Electron-Doped Cuprate Superconductors, *Phys. Rev. Lett.* **94**, 057005 (2005).
- [23] X. Zhou, D. C. Peets, Benjamin Morgan, W. A. Huttema, N. C. Murphy, E. Thewalt, C. J. S. Truncik, P. J. Turner, A. J. Koenig, J. R. Waldram, A. Hosseini, Ruixing Liang, D. A. Bonn, W. N. Hardy, and D. M. Broun, Logarithmic Upturn in Low-Temperature Electronic Transport as a Signature of d-Wave Order in Cuprate Superconductors, *Phys. Rev. Lett.* **121**, 267004 (2018).
- [24] K. Segawa, and Y. Ando, Charge localization from local destruction of antiferromagnetic correlation in Zn-doped YBa₂Cu₃O_{7-δ}, *Phys. Rev. B* **59**, R3948 (1999).
- [25] P. Fournier, J. Higgins, H. Balci, E. Maiser, C. J. Lobb, and R. L. Greene, Anomalous saturation of the phase coherence length in underdoped Pr_{2-x}Ce_xCuO₄ thin films, *Phys. Rev. B* **62**, R11 994 (2000).
- [26] F. Rullier-Albenque, H. Alloul, and R. Tourbot, Disorder and Transport in Cuprates: Weak Localization and Magnetic Contributions, *Phys. Rev. Lett.* **87**, 157001(2001).

- [27] M. Hepting, D. Li, C. J. Jia, H. Lu, E. Paris, Y. Tseng, X. Feng, M. Osada, E. Been, Y. Hikita, Y.-D. Chuang, Z. Hussain, K. J. Zhou, A. Nag, M. Garcia-Fernandez, M. Rossi, H. Y. Huang, D. J. Huang, Z. X. Shen, T. Schmitt, H. Y. Hwang, B. Moritz, J. Zaanen, T. P. Devereaux, and W. S. Lee, Electronic structure of the parent compound of superconducting infinite-layer nickelates, *Nat. Mater.* **19**, 381-385 (2020).
- [28] J. Y. Yang, Y. L. Han, L. He, R. F. Dou, C. M. Xiong, and J. C. Nie, D carrier induced intrinsic room temperature ferromagnetism in Nb:TiO₂ film, *Appl. Phys. Lett.* **100**, 202409 (2012).
- [29] C. M. Hurd, *The Hall Effect in Metals and Alloys*, (Plenum, New York, 1972).
- [30] See Supplemental Material for details, which includes references [48-58].
- [31] W. Felsch, and K. Winzer, Magnetoresistivity of (La, Ce)A₁₂ Alloys, *Solid State Commun.* **13**, 569 (1973).
- [32] A. Fert, and P. M. Levy, Theory of the Hall effect in heavy-fermion compounds, *Phys. Rev. B* **36**, 1907-1916 (1987).
- [33] N. Nagaosa, J. Sinova, S. Onoda, A. H. MacDonald, and N. P. Ong, Anomalous Hall effect, *Rev. Mod. Phys.* **82**, 1539-1592 (2010).
- [34] P. A. Lee, and T. V. Ramakrishnan, Disordered electronic systems, *Rev. Mod. Phys.* **57**, 287-337 (1985).
- [35] S. Hikami, A. I. Larkin, and Y. Nagaoka, Spin-Orbit Interaction and Magnetoresistance in the Two-Dimensional Random System, *Prog. Theor. Phys.* **63**, 707-710 (1980).
- [36] T. Micklitz, A. Altland, T. A. Costi, and A. Rosch, Universal Dephasing Rate due to Diluted Kondo Impurities, *Phys. Rev. Lett.* **96**, 226601 (2006).
- [37] R. P. Peters, G. Bergmann, and R. M. Mueller, Kondo Maximum of Magnetic Scattering, *Phys. Rev. Lett.* **58**, 1964-1967 (1987).
- [38] C. V. Haesendonck, J. Vranken, and Y. Bruynseraede, Resonant Kondo Scattering of Weakly Localized Electrons, *Phys. Rev. Lett.* **58**, 1968-1971 (1987).
- [39] J. Schoenes, and J. J. M. Franse, Hall effect in the heavy-fermion superconductor UPT₃, *Phys. Rev. B* **33**, 5138-5140 (1986).
- [40] J. Karp, A. S. Botana, M. R. Norman, H. Park, M. Zingl, and A. Millis, *Phys. Rev. X* **10**, 021061 (2020).
- [41] M. Osada, B. Y. Wang, B. H. Goodge, S. P. Harvey, K. Lee, D. Li, L. F. Kourkoutis, and H. Y. Hwang, Nickelate Superconductivity without Rare-Earth Magnetism: (La,Sr)NiO₂, *Adv. Mater.* **33**, 2104083 (2021).
- [42] Z. Liu, Z. Ren, W. Zhu, Z. Wang, and J. Yang, Electronic and magnetic structure of infinite-layer NdNiO₂: trace of antiferromagnetic metal, *npj Quantum Materials* **5**, 31 (2020).
- [43] Y. Gu, S. Zhu, X. Wang, J. Hu, and H. Chen, A substantial hybridization between correlated Ni-d orbital and itinerant electrons in infinite-layer nickelates, *Commun. Phys.* **3**, 84 (2020).
- [44] H. Lu, M. Rossi, A. Nag, M. Osada, D. F. Li, K. Lee, B. Y. Wang, M. Garcia-Fernandez, S. Agrestini, Z. X. Shen, E. M. Been, B. Moritz, T. P. Devereaux, J. Zaanen, H. Y. Hwang, Ke-Jin Zhou, and W. S. Lee, Magnetic excitations in infinite-layer nickelates, *Science* **373**, 213 – 216 (2021).
- [45] Y. Cui, C. Li, Q. Li, X. Zhu, Z. Hu, Y. Yang, J. Zhang, R. Yu, H.-H. Wen, and W. Yu, NMR Evidence of Antiferromagnetic Spin Fluctuations in *Nd_{0.85}Sr_{0.15}NiO₂*, *Chin. Phys. Lett.* **38**, 067401 (2021).
- [46] Y.-T. Hsu, B. Y. Wang, M. Berben, D. Li, K. Lee, C. Duffy, T. Ottenbros, W. J. Kim, M. Osada, S. Wiedmann, H. Y. Hwang, and Nigel E. Hussey, Insulator-to-metal crossover near the edge of the superconducting dome in NiNd_{1-x}Sr_xNiO₂, *Phys. Rev. Research* **3**, L042015 (2021).
- [47] K. Lee, B. Y. Wang, M. Osada, B. H. Goodge, T. C. Wang, Y. Lee, S. Harvey, W. J. Kim, Y. Yu, C. Murthy, S. Raghu, L. F. Kourkoutis, and Harold Y. Hwang, Character of the "normal state" of the nickelate superconductors, arXiv:2203.02580.

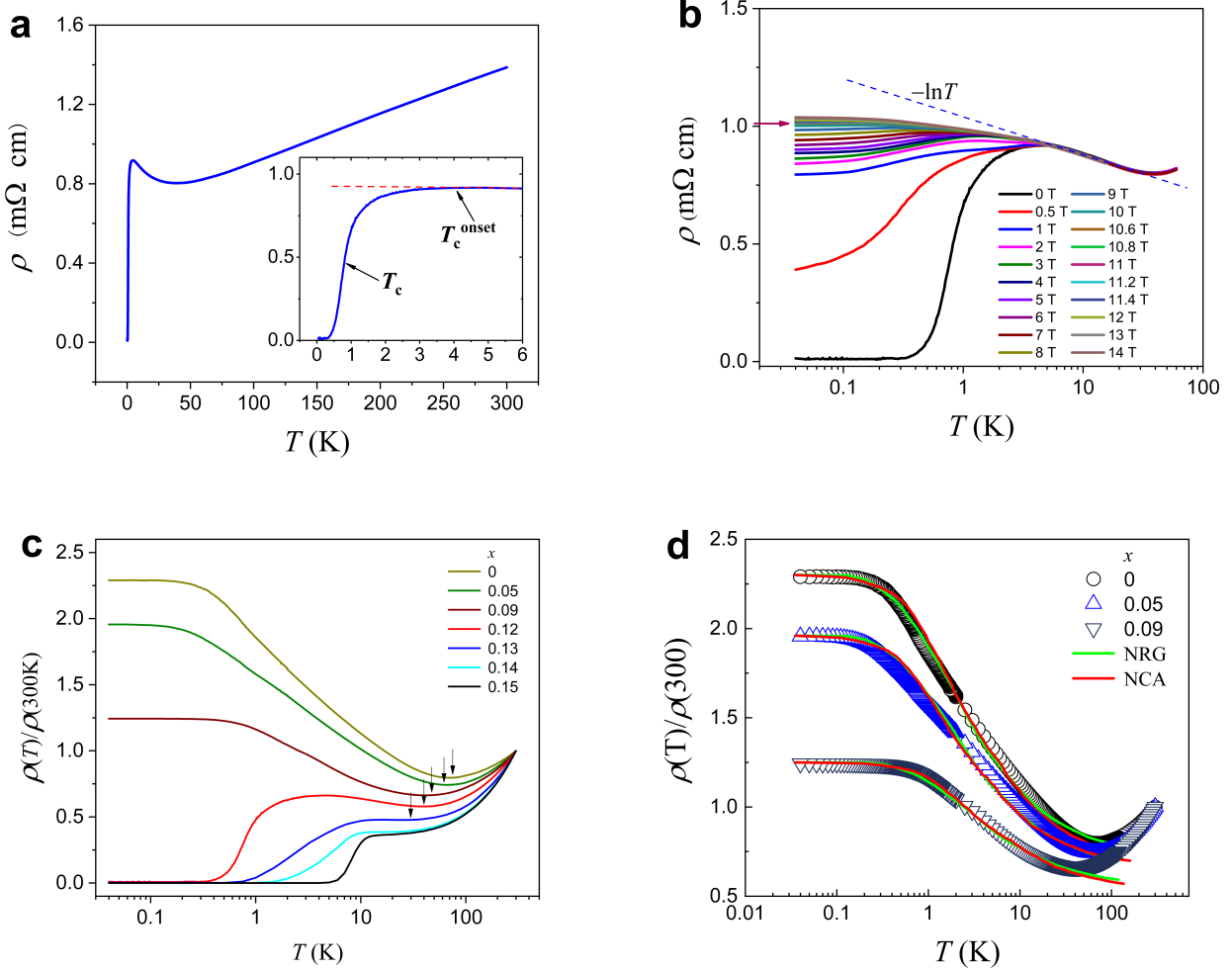


Fig. 1 | Temperature-dependent resistivity $\rho(T)$ for the underdoped $\text{Nd}_{1-x}\text{Sr}_x\text{NiO}_2$ thin films. **a, The temperature dependence of resistivity of the $\text{Nd}_{0.88}\text{Sr}_{0.12}\text{NiO}_2$ film at zero magnetic field. T_c and T_c^{onset} , marked by black arrows, are 0.79 K and 4.06 K, respectively. The inset shows the determination of T_c^{onset} . **b**, Isomagnetic $\rho(T)$ curves of the $\text{Nd}_{0.88}\text{Sr}_{0.12}\text{NiO}_2$ film measured at different applied magnetic field H . **c**, The zero-field temperature dependence of resistivity of the underdoped $\text{Nd}_{1-x}\text{Sr}_x\text{NiO}_2$ films with a Sr doping level x from 0.00 to 0.15. The arrows indicate the corresponding resistivity minima. **d**, The NRG (green) and NCA (red) fits are shown for the underdoped samples with $x = 0, 0.05,$ and $0.09,$ and $T_K = 3.5 \text{ K}, 3.5 \text{ K}$ and $5.5 \text{ K},$ respectively (see details in Supplementary Fig. 4).**

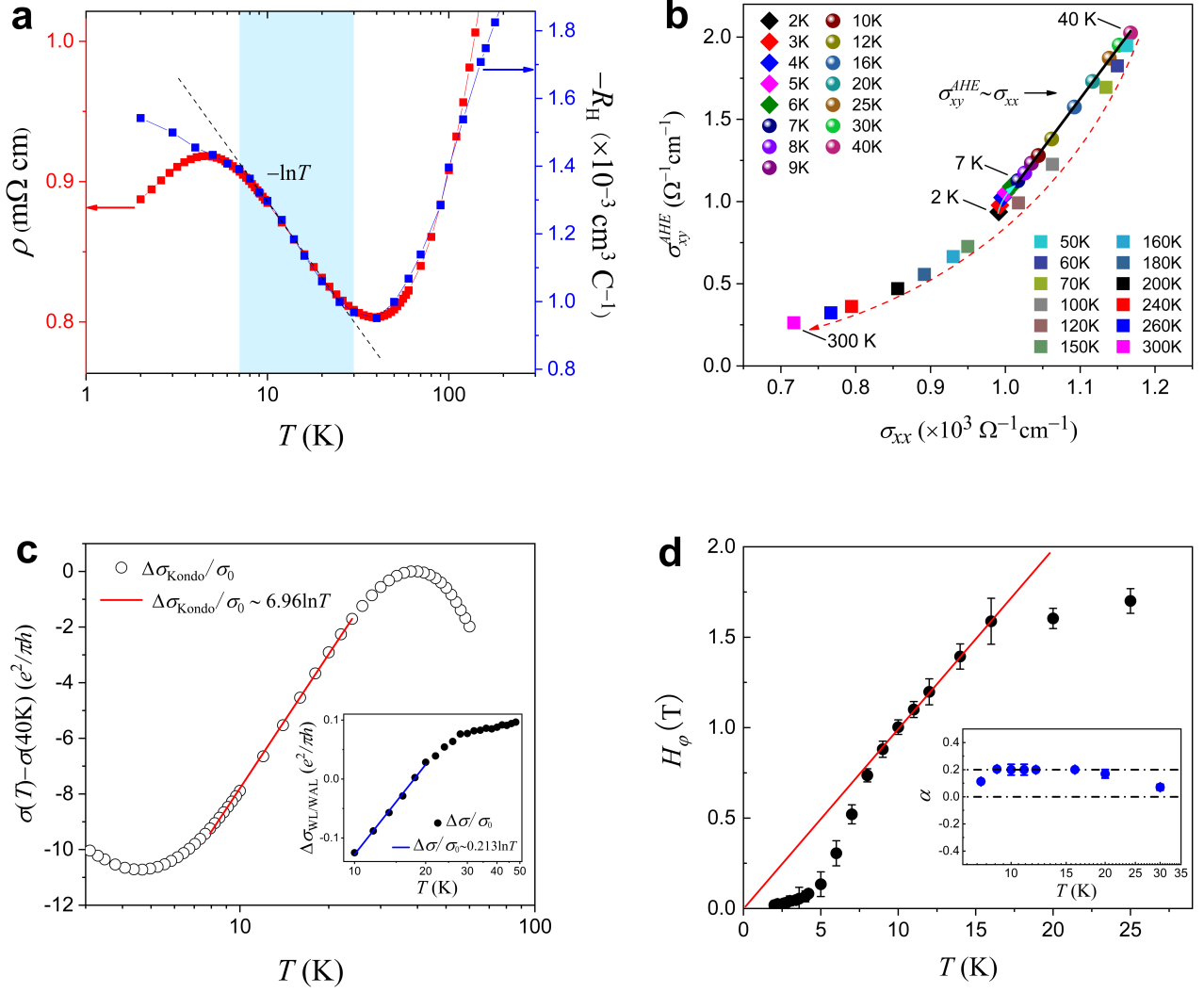


Fig. 2 | Scaling behavior of anomalous Hall conductivity and conductance corrections for $\text{Nd}_{0.88}\text{Sr}_{0.12}\text{NiO}_2$. **a**, Logarithmic temperature dependence of the resistivity (red) and the Hall coefficient (blue) of the $\text{Nd}_{0.88}\text{Sr}_{0.12}\text{NiO}_2$ film. The light cyan area represents the Kondo region. **b**, Plot of AHE conductivity σ_{xy}^{AHE} vs conductivity σ_{xx} of the $\text{Nd}_{0.88}\text{Sr}_{0.12}\text{NiO}_2$ film over the entire temperature range. Since $\rho_{xy} \sim \rho_{xx}/10^3$, we can simplify the anomalous Hall conductivity as $\sigma_{xy}^{AHE} = -\rho_{xy}^{AHE}/\rho_{xx}^2$, and here $\rho_{xy}^{AHE} \equiv (R_H - R_0) \cdot H$. A linear dependence (solid black line) of $\sigma_{xy}^{AHE} \sim \sigma_{xx}$ is obvious in a temperature range of 7–40 K. **c**, Zero field conductance correction for the $\text{Nd}_{0.88}\text{Sr}_{0.12}\text{NiO}_2$ film due to the Kondo effect, i.e., $\Delta\sigma_{Kondo} = \sigma(T) - \sigma(T_{min} = 40\text{K})$. Data are extracted from Fig. 1b and the solid red line is the $\ln T$ fits. Inset: Conduction correction due to the WL/WAL effect, which is obtained with $\Delta\sigma_{WL/WAL} = \sigma(T)|_{H=0} - \sigma(T)|_{H=4T}$ (solid circles). The solid blue line is the $\ln T$ fit for obtaining $\Delta\kappa = \alpha p$, and here $\sigma_0 = e^2/\pi h$. **d**, Dephasing field H_ϕ versus temperature for the $\text{Nd}_{0.88}\text{Sr}_{0.12}\text{NiO}_2$ film. The straight red line is the linear fit. The inset shows the corresponding α values, which are nearly constant in the temperature range of 9–20 K.

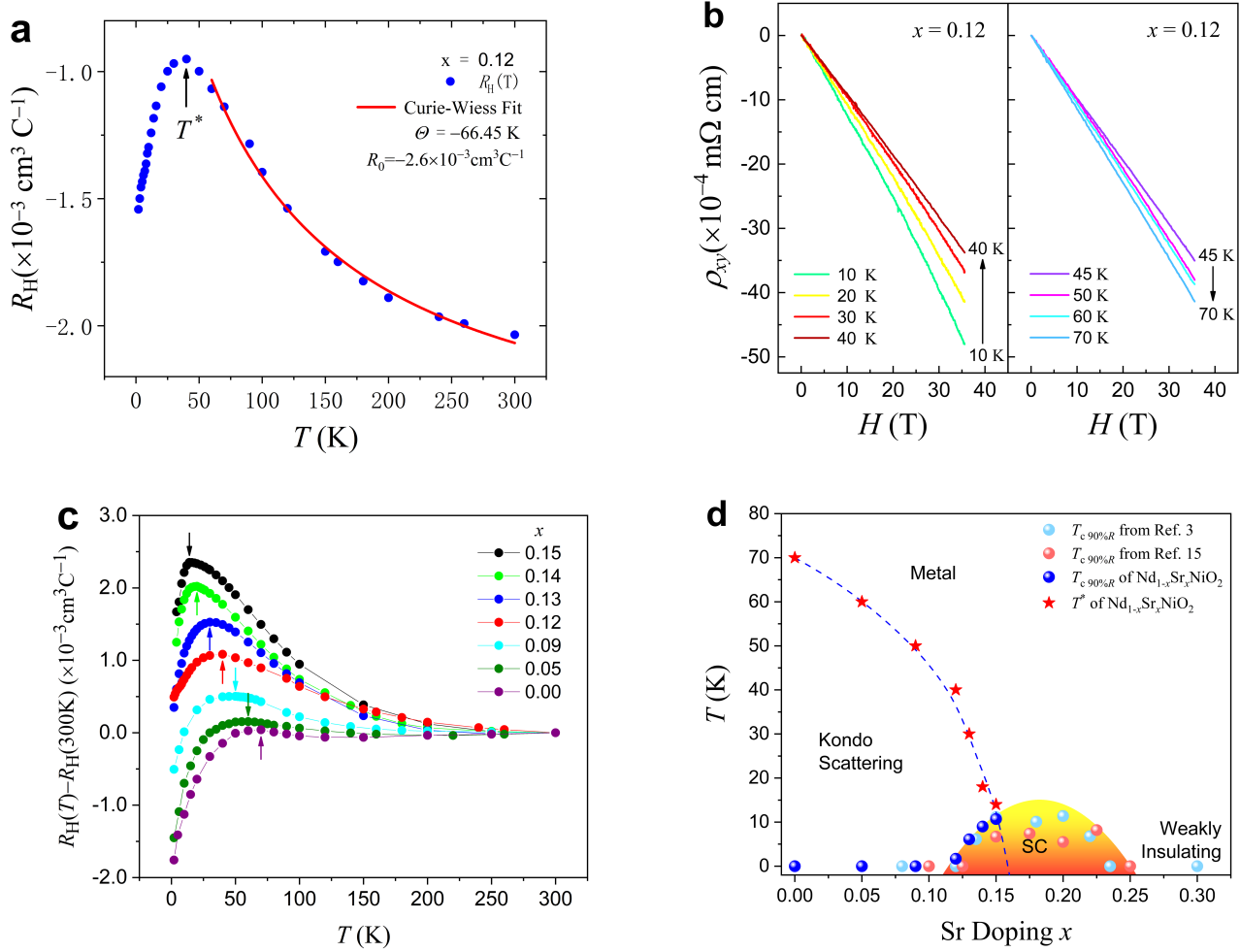


Fig. 3 | Kondo scattering dominated region in phase diagram of $\text{Nd}_{1-x}\text{Sr}_x\text{NiO}_2$. **a**, Hall coefficient $R_H(T)$ acquired in a field of 9 T for the $\text{Nd}_{0.88}\text{Sr}_{0.12}\text{NiO}_2$ film with a maximum around 40 K. **b**, Measured Hall resistivity, ρ_{xy} , versus magnetic field, H , at different temperatures. The Hall resistivity ρ_{xy} shows no obvious deviation from linear dependence on magnetic field H up to 35 T at all temperatures. **c**, Hall coefficient $R_H(T) - R_H(300\text{K})$ acquired in a field of 9 T for the underdoped $\text{Nd}_{1-x}\text{Sr}_x\text{NiO}_2$ films, with a maximum around T^* , at which the resistivity normally shows a minimum (see the arrows in Fig.1c). The corresponding characteristic temperatures T^* are indicated by the arrows. **d**, The superconducting transition temperature T_c (circles) and the characteristic temperature T^* (stars) where the R_H shows a maximum (Fig. 3c). The $T_{c90\%R}$ is defined to be the temperature at which the resistivity drops to 90% of the value at the onset of the superconductivity. The cyan and orange circles represent the average $T_{c90\%R}$ adapted from references [3,15]. The blue circles represent the $T_{c90\%R}$ of the samples shown in this study.

Supplementary Material

Kondo scattering in underdoped $\text{Nd}_{1-x}\text{Sr}_x\text{NiO}_2$ infinite-layer superconducting thin films

T. N. Shao¹, Z. T. Zhang¹, Y. J. Qiao¹, Q. Zhao¹, H. W. Liu^{1*}, X. X. Chen¹, W. M. Jiang¹, C. L. Yao¹, X. Y. Chen¹, M. H. Chen¹, R. F. Dou¹, C. M. Xiong¹, G. M. Zhang^{2,3*}, Y.-F. Yang^{4,5,6*}, J. C. Nie^{1*}

¹*Department of Physics, Beijing Normal University, Beijing 100875, China*

²*State Key Laboratory of Low-Dimensional Quantum Physics and Department of Physics, Tsinghua University, Beijing 100084, China*

³*Frontier Science Center for Quantum Information, Beijing 100084, China*

⁴*Beijing National Laboratory for Condensed Matter Physics and Institute of Physics, Chinese Academy of Sciences, Beijing 100190, China*

⁵*School of Physical Sciences, University of Chinese Academy of Sciences, Beijing 100190, China*

⁶*Songshan Lake Materials Laboratory, Dongguan, Guangdong 523808, China*

*Corresponding author. E-mail: jcnie@bnu.edu.cn (J.C.N.); yifeng@iphy.ac.cn (Y.-F.Y.); gmzhang@tsinghua.edu.cn (G.M.Z.); haiwen.liu@bnu.edu.cn (H.W.L.)

Methods

Sample preparation and characterization

The $\text{La}_{1-x}\text{Sr}_x\text{NiO}_3$ target was prepared by a stoichiometric mixture of SrCO_3 , Nd_2O_3 , and NiO powders used a solid-state reaction in air at 1350°C for 12 hours. The products were ground and reheated of this reaction, and this process was repeated three times. The powder was pressed into 2.5cm sheets and then calcined for 24 h at 1200°C in air. The heating and cooling of the sintering were kept at a rate of $10^\circ\text{C}/\text{min}$. Precursor perovskite thin films were grown on the TiO_2 -terminated SrTiO_3 substrate (NH_4F buffered HF etching solution) by pulsed laser deposition from polycrystalline target ablated with a KrF excimer laser (wavelength = 248 nm). During the deposition, the oxygen partial pressure was 150 mTorr and the substrate temperature was at 600°C . After deposition, the films were kept at 600°C for 10 minute and cooled to room temperature at a rate of 10°C per minute in the same oxygen partial pressure. The laser energy was $1.2\text{ J}/\text{cm}^2$ and the frequency was 4 Hz. For the very thin as-grown films less than 10 nm, nominal thickness was usually determined by the number of laser shots and the calibrated growth rate [48]. The soft-chemistry reduction method [1,3,7,41,49,50] was used to acquire the infinite-layer nickelate phase. The as-grown precursor perovskite thin films were placed in Pyrex glass tubes with calcium hydride (CaH_2) powder ($\sim 0.1\text{ g}$) after loosely wrapping them with aluminum foil. The glass tubes were pumped to a vacuum about 1×10^{-5} Torr. Then it was heated up to 320°C and keep for 2 hours, with the heating and cooling rates of $10^\circ\text{C}/\text{min}$.

The structural properties of the films were measured by using a x-ray diffractometer (Shimadzu XRD-6000). The valence state and the atomic ratio of the relevant elements of the reduced sample was investigated by a Thermo Scientific ESCSLAB 250Xi XPS. For very thin as-grown films, the mean grain size (out-of-plane) d is well consistent with the film thickness. The full width at half maximum (FWHM) of the most intense XRD peaks, (002) of the perovskite $\text{Nd}_{1-x}\text{Sr}_x\text{NiO}_3$ and (002) of the infinite-layer $\text{Nd}_{1-x}\text{Sr}_x\text{NiO}_2$, are routinely used to

determine d using the Scherrer formula, $d=(0.9\lambda/\beta_c\cos\theta)$, where λ is the wavelength of the filament used in the XRD machine, β_c is the FWHM, θ is the angle of the same peak.

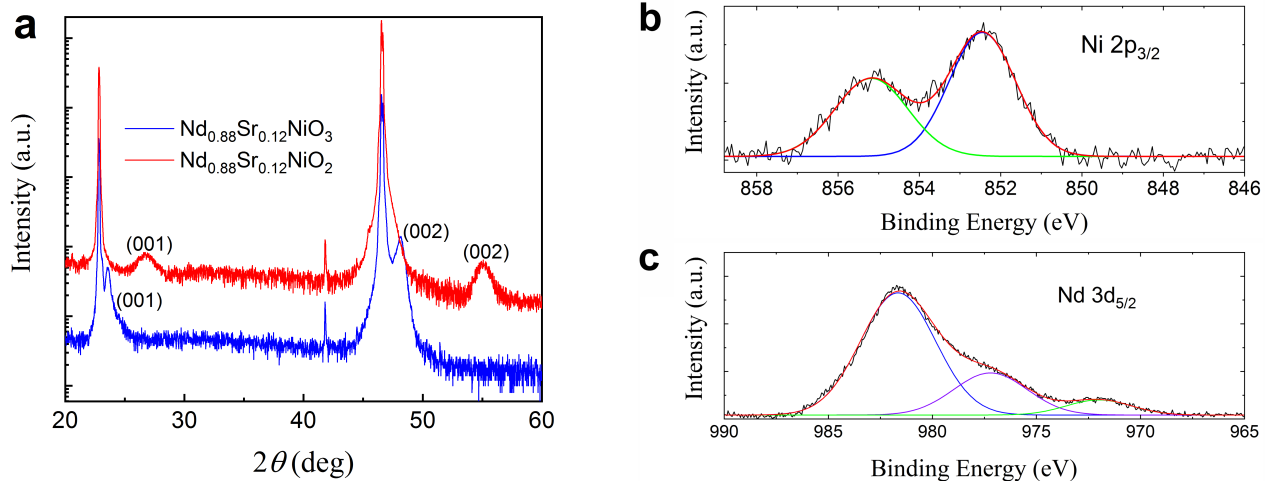
Electrical Measurements

The normal state electrical-transport and magneto-transport measurements were carried out using the Van der Pauw configuration in a physical property measurement system (PPMS, Quantum Design). Electrode contacts to the samples were bonded by ultrasonic wire bonding (Al wire of 25 μm diameter). The DC current for the normal state measurements was 10 μA . The sub-Kelvin measurements were performed with a lock-in amplifier (Stanford Research System, SR830) in AC mode in a dilution refrigerator Triton-400 system (Oxford Instruments, base temperature < 10 mK). Standard four probe resistance measurements were made with sufficiently low excitation current (50 nA at 7.9 Hz) to avoid any heating of the electrons at the lowest temperature. The high magnetic field (0-35 T) measurements were carried out by the Hefei Steady-state High Magnetic Field Facilities in High Magnetic Field Laboratory, Chinese Academy of Sciences and University of Science and Technology of China.

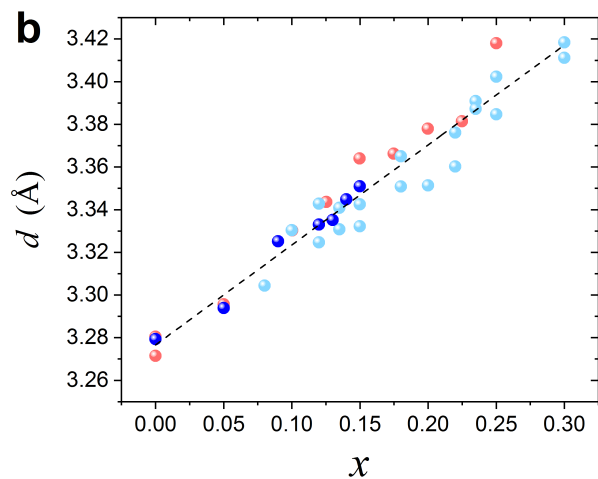
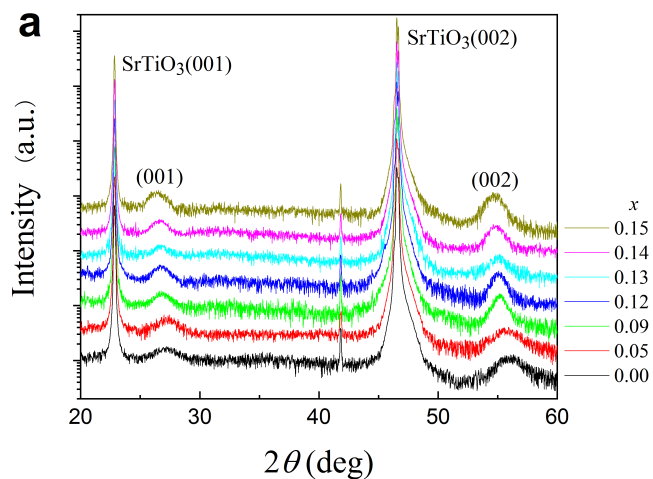
Results and Discussion

Supplementary Fig. 1a illustrates the structural properties of the representative $\text{Nd}_{1-x}\text{Sr}_x\text{NiO}_3$ thin films before the topotactic reduction, characterized by X-ray diffraction (XRD) measurements. The thickness of the as-grown film is about 8.48 nm. After chemical reduction, the film peaks appear at 26.70° and 55.06° , which are the characteristic peaks of the infinite layer $\text{Nd}_{1-x}\text{Sr}_x\text{NiO}_2$, corresponding to (001) and (002) reflections, respectively. The corresponding c-axis lattice constant is about 3.333 \AA , indicating a slight expansion of the c-axis lattice constant comparing with that (3.28 \AA) of the undoped NdNiO_2 film [15]. According to the previous reports [3,15], in our case, the empirical Sr doping level x is about 0.12, consistent with that of the stoichiometric target.

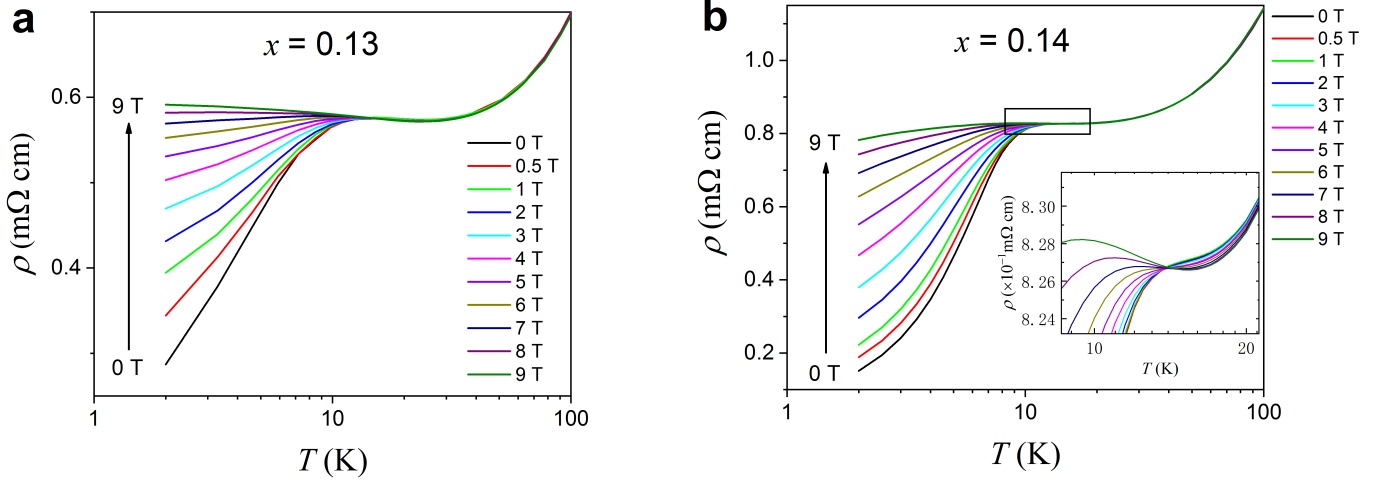
In order to further quantitatively analyze the chemical composition and elemental valence of the film, X-ray photoelectron spectroscopy (XPS) measurements were carried out. Supplementary Fig. 1b and Fig. 1c show the XPS spectra of Ni $2p_{3/2}$ and Nd $3d_{5/2}$ of the representative $\text{Nd}_{1-x}\text{Sr}_x\text{NiO}_2$ sample treated by the topotactic hydrogen reduction. The peak at the binding energy of 852.5 eV corresponds to Ni^+ cations, and the left side peak at the binding energies 854.6 eV originates from Ni^{2+} cations [51]. A quantitative analysis, as shown in Supplementary Fig. 1b, gives the relative concentrations of Ni^+ and Ni^{2+} cations. It turns out that the percentages of Ni^+ and Ni^{2+} cations are 71.8% and 28.2%, respectively. The high resolution XPS spectrum of Nd $3d_{5/2}$ core level line is displayed in Supplementary Fig. 1c. The main peak of Nd $3d_{5/2}$ at the binding energy of 982.2 eV corresponds to Nd^{3+} cations, and the one at 978.2 eV is a satellite peak of the main one, while the shoulder at low binding energy (972.7 eV) is expected to contain a significant contribution of the $\text{KL}_{23}\text{L}_{23}$ Auger of oxygen which is consistently observed in most oxides, such as Nd_2NiO_4 [52]. The calculated atomic ratio of Nd:Ni is about 0.884:1, which is well consistent with the result of the XRD data. Both the XRD and XPS results indicate that the composition of the representative infinite-layer thin film is $\text{Nd}_{0.88}\text{Sr}_{0.12}\text{NiO}_2$, which is in the underdoped region. In addition, a nickel oxidation state of +1.28 may indicate a little excess oxygen content in the infinite-layer thin film.



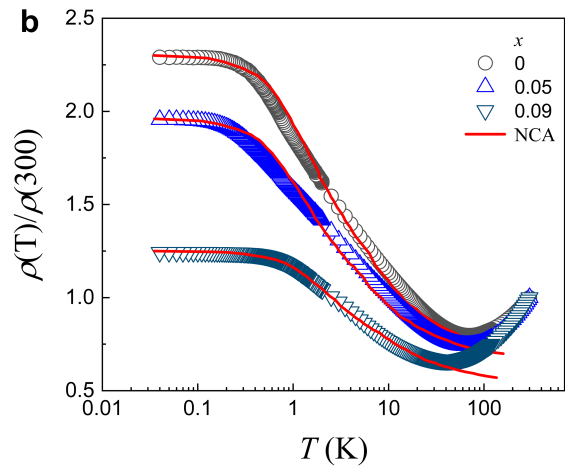
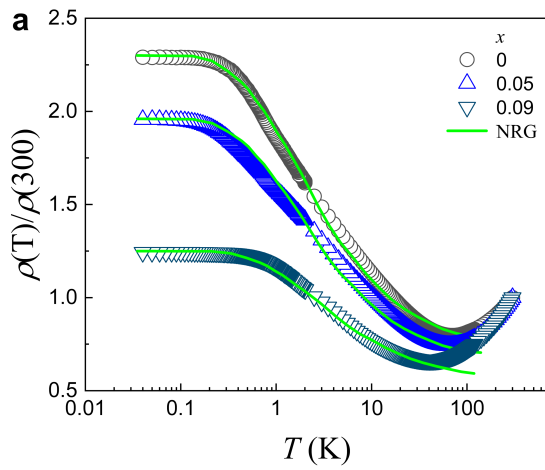
Supplementary Fig. 1 | Characterization of the representative nickelate thin film. (a) Structural characterization of the nickelate film on SrTiO_3 substrate. The XRD θ - 2θ scans of the representative $\text{Nd}_{0.88}\text{Sr}_{0.12}\text{NiO}_3$ film before and after the topotactic reduction at 320°C for 2 hours. XPS spectra of Ni 2p (b) and Nd 3d (c) of the representative $\text{Nd}_{0.88}\text{Sr}_{0.12}\text{NiO}_2$ sample treated by the topotactic hydrogen reduction.



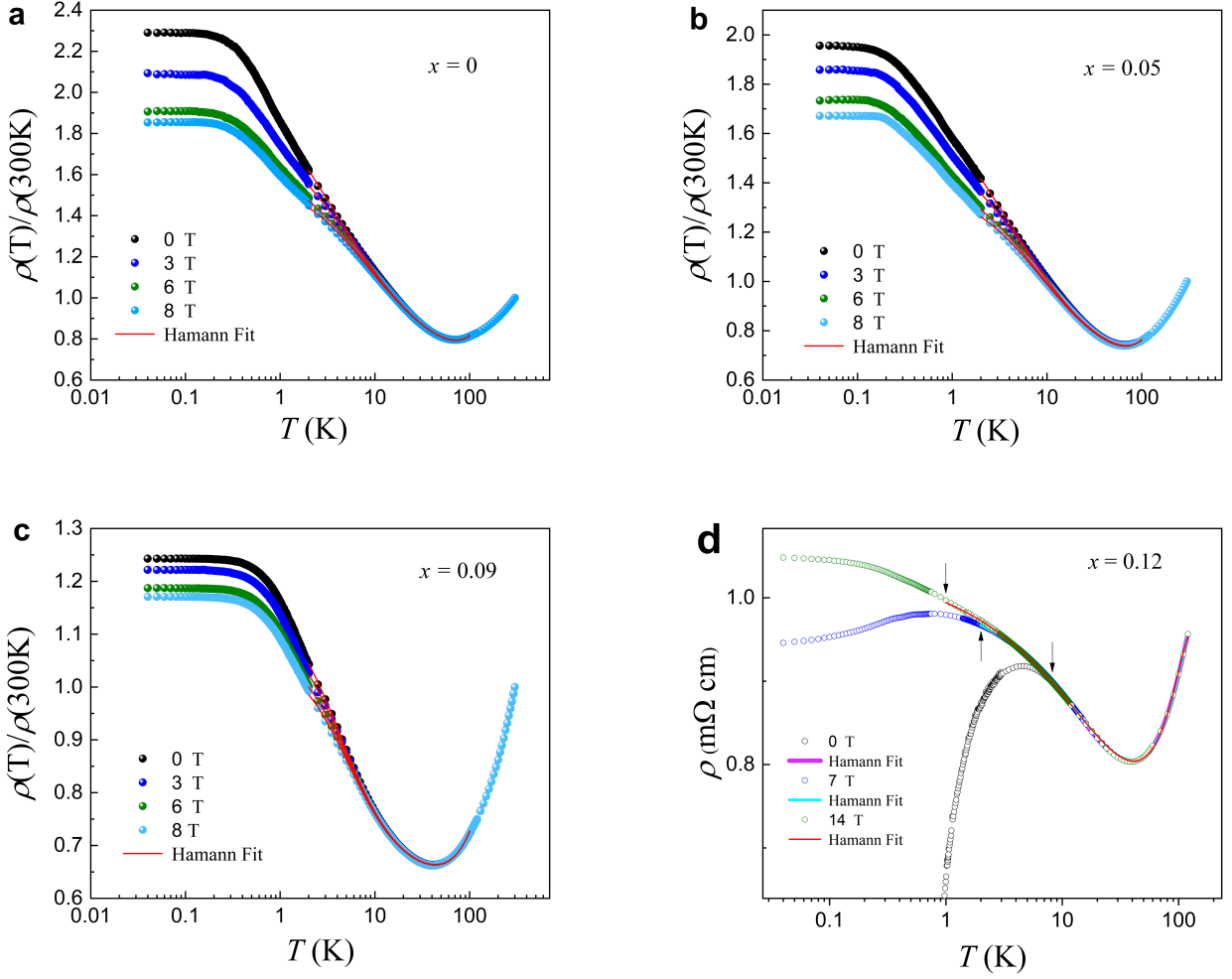
Supplementary Fig. 2 | Structural characterization of the underdoped $\text{Nd}_{1-x}\text{Sr}_x\text{NiO}_2$ infinite layer thin films with different Sr doping. (a) The XRD patterns of the underdoped $\text{Nd}_{1-x}\text{Sr}_x\text{NiO}_2$ infinite layer thin films. The intensity is vertically displaced for clarity. (b) Room-temperature c -axis lattice constants d as a function of Sr doping level x . The blue circles represent the data extracted from the θ - 2θ scans in (a) and the cyan and orange circles represent the data adapted from references [3,15]. The dashed line is a guide to the eye.



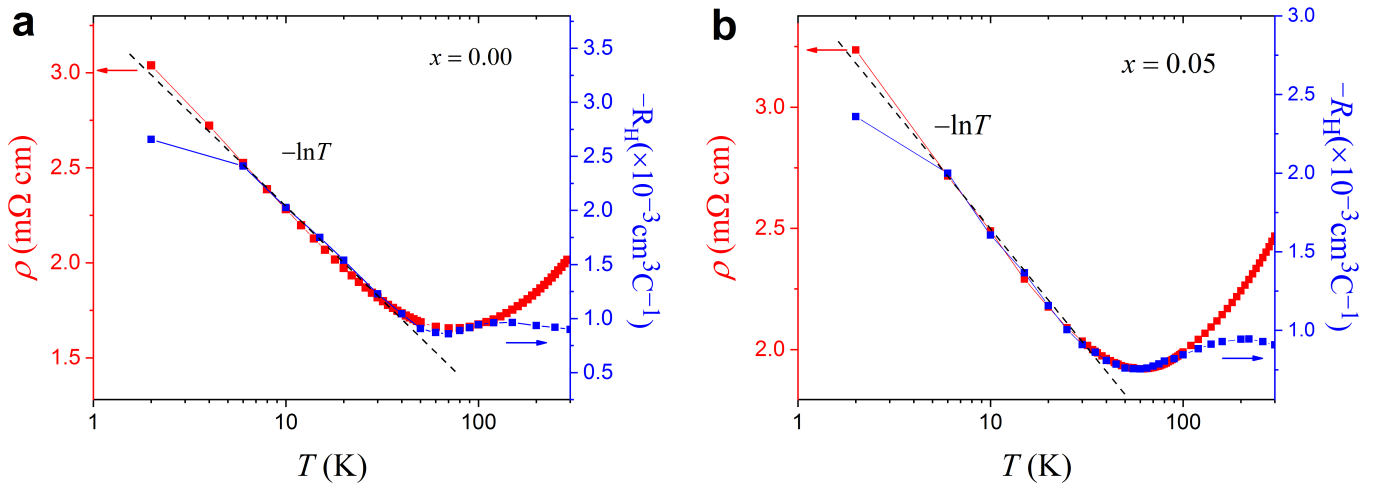
Supplementary Fig. 3 | Isomagnetic $\rho(T)$ curves of the other under-doped $\text{Nd}_{1-x}\text{Sr}_x\text{NiO}_2$ thin films with a Sr doping level $x = 0.13$ (a) and 0.14 (b). For the sample with $x = 0.13$ (a), in all magnetic fields, the resistivity-temperature curve shows a low-temperature minimum, followed by an upturn that is proportional to $\ln T$ with decrease of temperature. (b) For the sample with $x = 0.14$, in a strong magnetic field (e.g., $H > 7.0$ T), the resistivity-temperature curve shows a low-temperature minimum followed by a small upturn that is proportional to $\ln T$ with decrease of temperature (see the inset). The inset is an enlarged view of the block in Supplementary Fig. 3b.



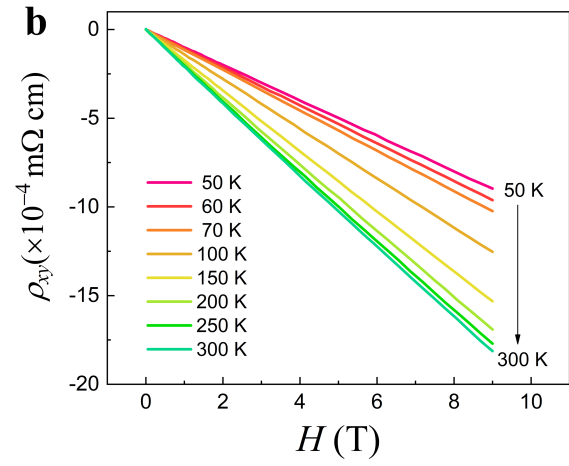
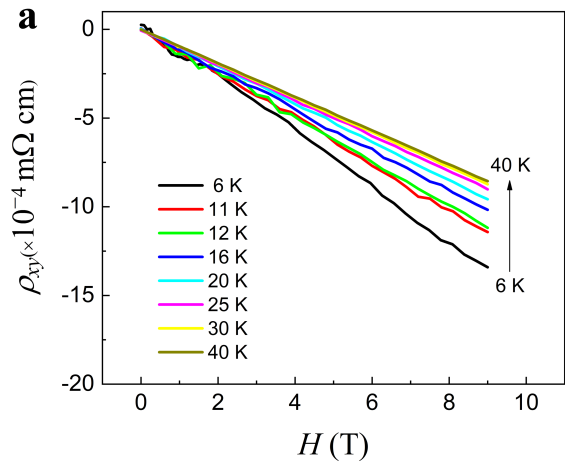
Supplementary Fig. 4 | Temperature dependence of resistivity of the underdoped $\text{Nd}_{1-x}\text{Sr}_x\text{NiO}_2$ film, fitted by NRG (a) and NCA (b) in temperature regime from 0.04 K to 100 K. The experimental data show the resistivity as a function of T from 0.04 K to 300 K. The fitting curves give $T_K = 3.5$ K, 3.5 K and 5.5 K for $x = 0, 0.05$ and 0.09 samples, respectively. The NCA fitting is compared with Fig.9.29 in Hewson's book [20]. The NRG fitting is compared with Fig.13 in the work by Costi et al. [20].



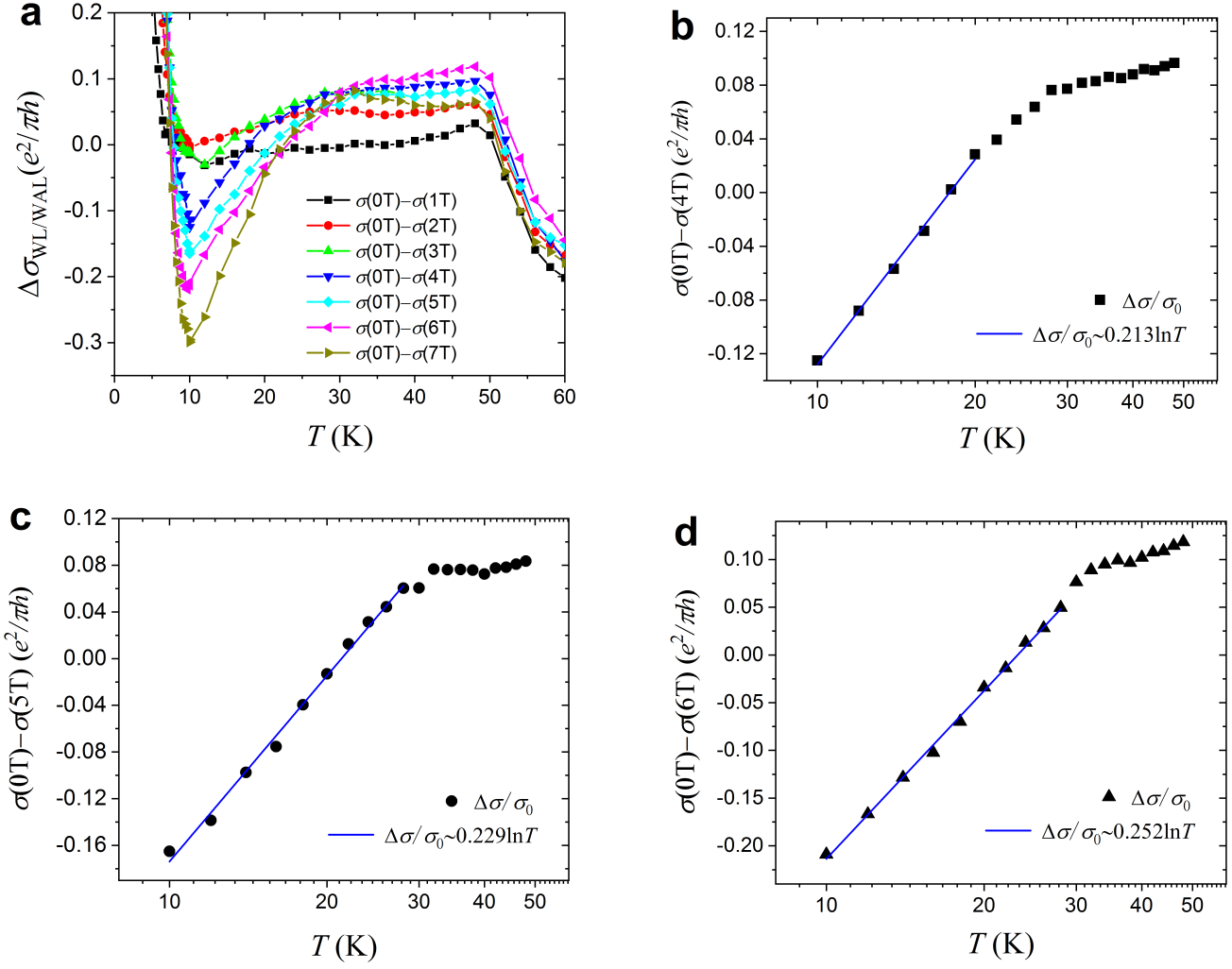
Supplementary Fig. 5 | Temperature dependence of resistivity of the underdoped $\text{Nd}_{1-x}\text{Sr}_x\text{NiO}_2$ film, fitted by Hamann Model. (a), (b) and (c) show the resistivity as a function of T from 0.04 K to 300 K for $x = 0, 0.05$ and 0.09 samples, respectively. The data without magnetic field are fitted by the Hamann model in temperature regime from 2 K to 100 K (Eq. 1 and Eq.2 in the main text), with the Kondo temperature $T_K = 3.5$ K, 4.0 K and 4.38 K and $s = 0.68, 0.59$ and 0.23 for $x = 0, 0.05$ and 0.09 samples, respectively. The data under magnetic field are fitted by the modified Hamann model [31]. Under magnetic field, the magnetoresistance can be obtained by the: $\rho_K(T/T_K) = \rho_0 \left\{ 1 - \frac{\ln(T/T_K)}{[\ln^2(T/T_K) + s(s+1)\pi^2]^{-1/2}} \right\} \cdot \left[1 - F^2 \left(\frac{g\mu_B H}{k_B(T+T_K)} \right) \right]$. Here, $F(x)$ is the Brillouin function for spin s and g denotes the Landé g -factor. Related discussions are shown in Supplementary Note 2. (d) shows the resistivity of the $x = 0.12$ sample as a function of T from 0.04 K to 120 K. Solid lines are fitting result using modified Hamann model, yielding the Kondo temperature T_K of about 15.6 K, the effective spin $s = 0.225$, and the magnetic impurity concentration c of about $5.83 \times 10^{20} \text{cm}^{-3}$, i.e., 0.03 magnetic-ion per unit cell in $\text{Nd}_{0.88}\text{Sr}_{0.12}\text{NiO}_2$, which is reasonable and comparable with that of dilute Kondo systems [29, 30].



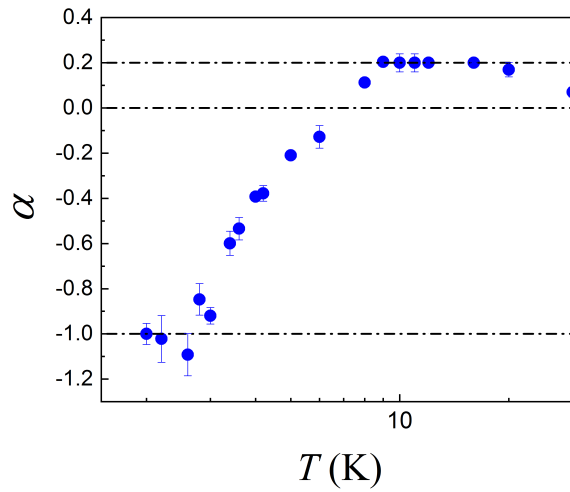
Supplementary Fig. 6 | Logarithmic temperature dependence of the zero-field resistivity and the Hall coefficient of the other under-doped $\text{Nd}_{1-x}\text{Sr}_x\text{NiO}_2$ thin films with (a) $x=0.00$ and (b) $x=0.05$. For the underdoped nickelates, the R_H resembles the $\ln T$ dependence of the resistivity for temperatures in a wide temperature range. The deviation of $R_H(T)$ from the $\ln T$ dependence at the lowest temperatures is obvious.



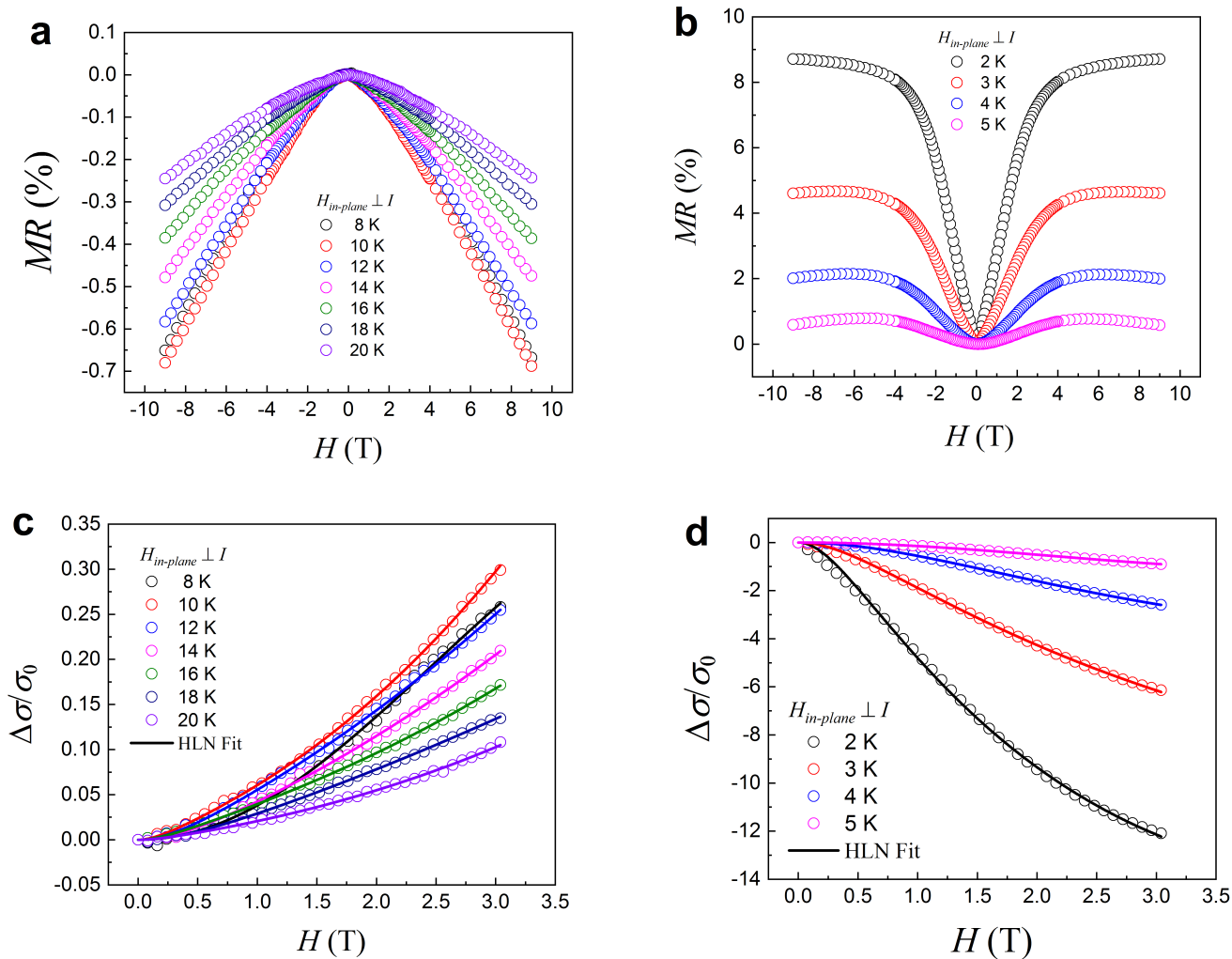
Supplementary Fig. 7 | Field dependence of Hall resistivity of the representative $\text{Nd}_{0.88}\text{Sr}_{0.12}\text{NiO}_2$ film. Measured Hall resistivity, ρ_{xy} , versus magnetic field, H , at different temperatures: (a) 6–40 K and (b) 50–300 K. The Hall resistivity ρ_{xy} shows no obvious deviation from linear dependence on magnetic field H up to 9 T at all temperatures.



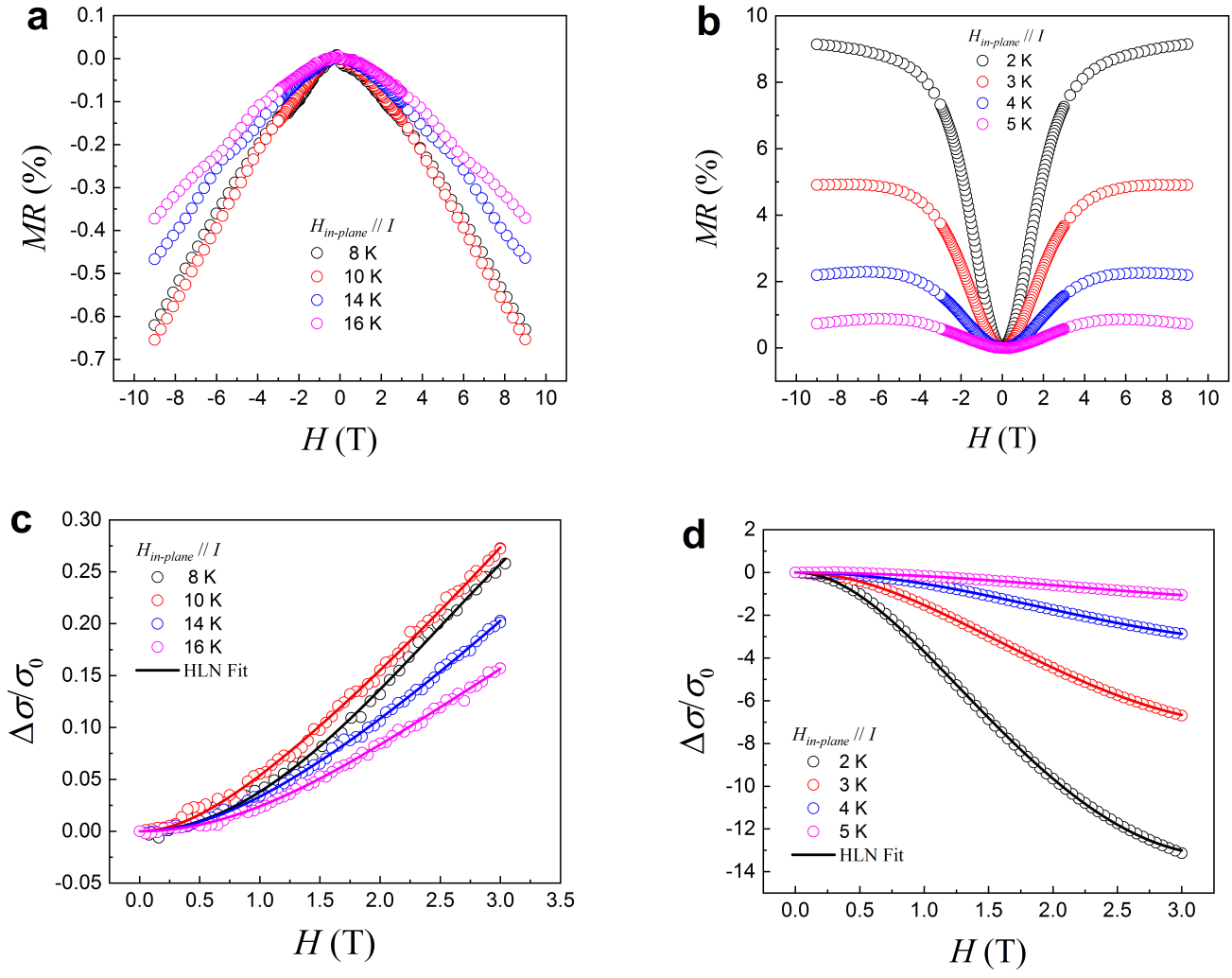
Supplementary Fig. 8 | WAL corrections of conductivity of the representative $\text{Nd}_{0.88}\text{Sr}_{0.12}\text{NiO}_2$ film. The WL/WAL effect is insignificant at higher magnetic fields, the conductivity correction $\Delta\sigma_{\text{WL/WAL}} = \sigma(T)|_{H=0} - \sigma(T)|_{H=4T}$ represents the WL/WAL correction [53]. (a) Conduction corrections due to the WAL effect, which are obtained with $\Delta\sigma_{\text{WL/WAL}} = \sigma(T)|_{H=0} - \sigma(T)|_{H \neq 0}$. Logarithmic temperature dependence of conduction correction in a range of 10–48 K, with $\Delta\sigma_{\text{WL/WAL}} = \sigma(T)|_{H=0} - \sigma(T)|_{H=4T}$. (b), $\Delta\sigma_{\text{WL/WAL}} = \sigma(T)|_{H=0} - \sigma(T)|_{H=5T}$ (c), and $\Delta\sigma_{\text{WL/WAL}} = \sigma(T)|_{H=0} - \sigma(T)|_{H=6T}$ (d), respectively. The solid lines are the $\ln T$ fits for obtaining $\Delta\kappa = \alpha p$. As shown in Supplementary Fig. 7, $\alpha \approx 0.20$ can be maintained for a wide temperature range of 10–20 K. Thus, one can also obtain H_ϕ have a linear power-law dependence satisfying $H_\phi \sim T^p$ with $p \approx 1$, which is consistent with the analysis of HLN formula in Fig.2d.



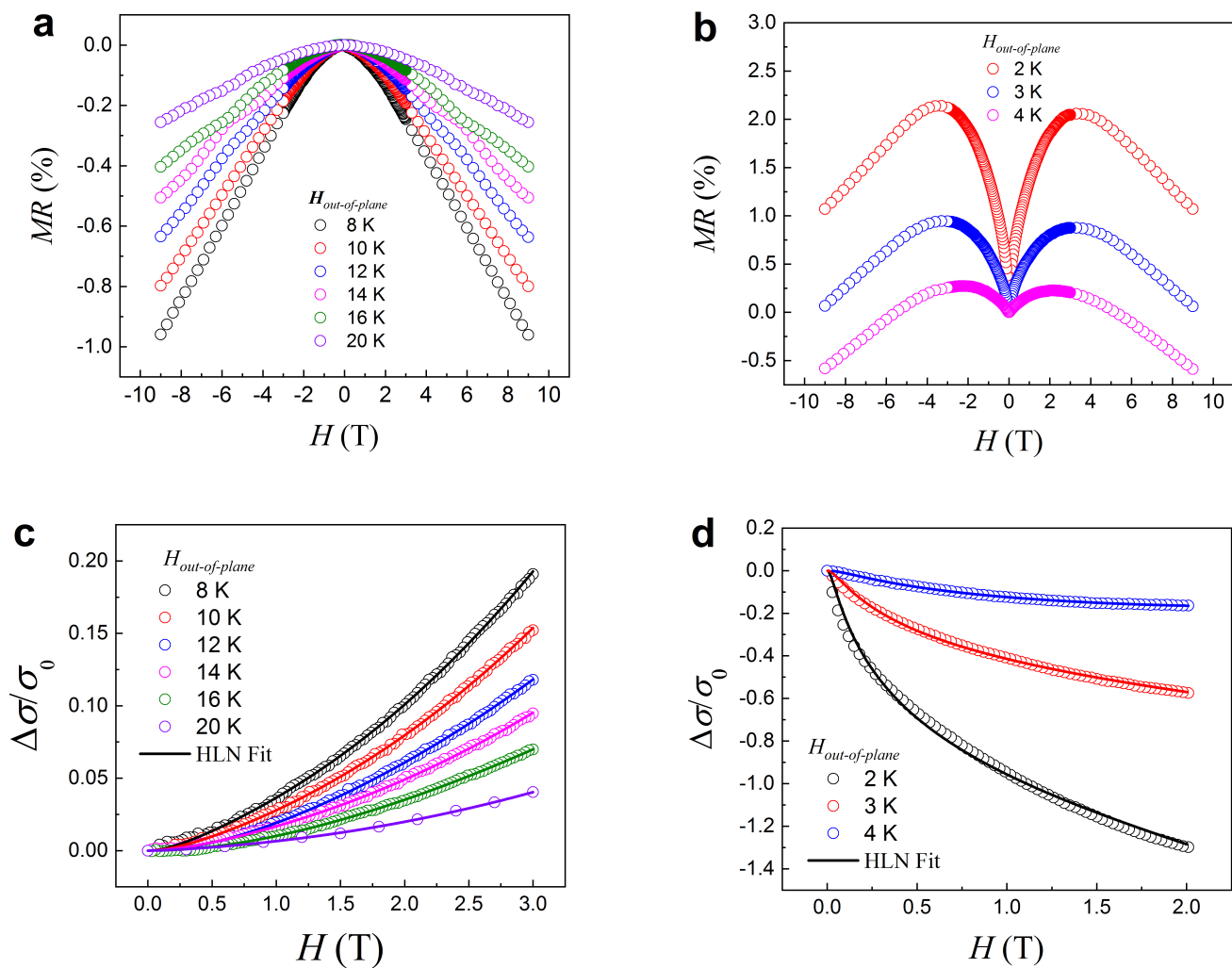
Supplementary Fig. 9 The α values of the HLN fitting for the representative $\text{Nd}_{0.88}\text{Sr}_{0.12}\text{NiO}_2$ film. A small value of $\alpha \approx 0.20$ can be maintained for a wide temperature range of 10–20 K. Here, α is an effective constant in the modified Hikami-Larkin-Nagaoka formula, which depends on the relative strengths of magnetic scattering and spin-orbital coupling. Typically, e.g., $\alpha = 1$ for weak spin-orbit and magnetic scattering, $\alpha = -1/2$ for strong SOC and weak magnetic scattering, and $\alpha = 0$ for strong magnetic scattering.



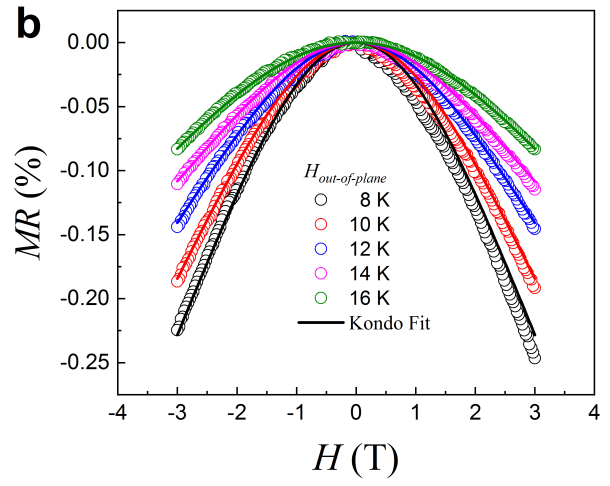
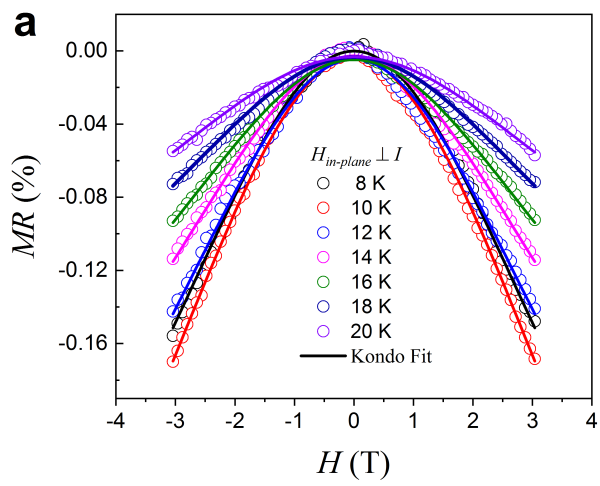
Supplementary Fig. 10 | In-plane transverse MR_{\perp} of the representative $\text{Nd}_{0.88}\text{Sr}_{0.12}\text{NiO}_2$ film, fitted by HLN. MR_{\perp} ($H \parallel ab$, $H \perp I$), at temperatures of 8–20 K (a) and 2–5 K (b). A sign change in MR_{\perp} is seen below 7 K. (c) $\Delta\sigma/\sigma_0$ as a function of H at high temperatures. (d) $\Delta\sigma/\sigma_0$ as a function of H at low temperatures. The solid curves are fitting to the HLN Eq. (3) in the main text, by adding a H^2 term.



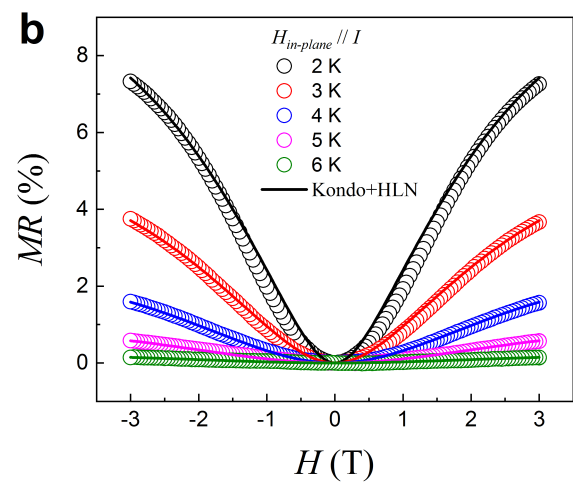
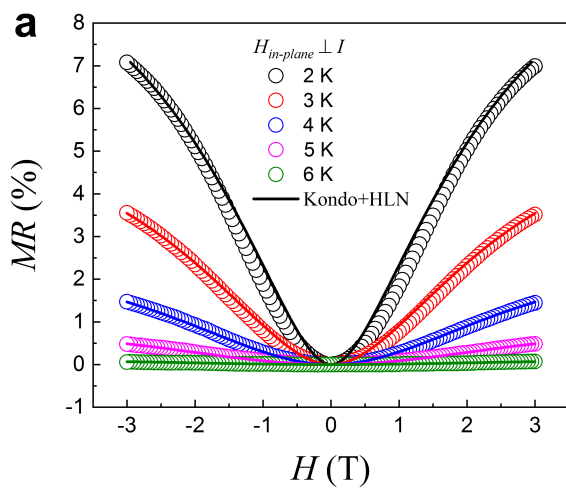
Supplementary Fig. 11 | In-plane longitudinal $MR'_{//}$ of the representative $\text{Nd}_{0.88}\text{Sr}_{0.12}\text{NiO}_2$ film, fitted by HLN. In-plane longitudinal $MR'_{//}$ ($H//ab$, $H//I$), at temperatures of 8–16 K (a) and 2–6 K (b). A sign change in $MR'_{//}$ is seen below 7 K. (c) $\Delta\sigma/\sigma_0$ as a function of H at high temperatures. (d) $\Delta\sigma/\sigma_0$ as a function of H at low temperatures. The solid curves are fitting to the HLN Eq. (3) in the main text, by adding a H^2 term.



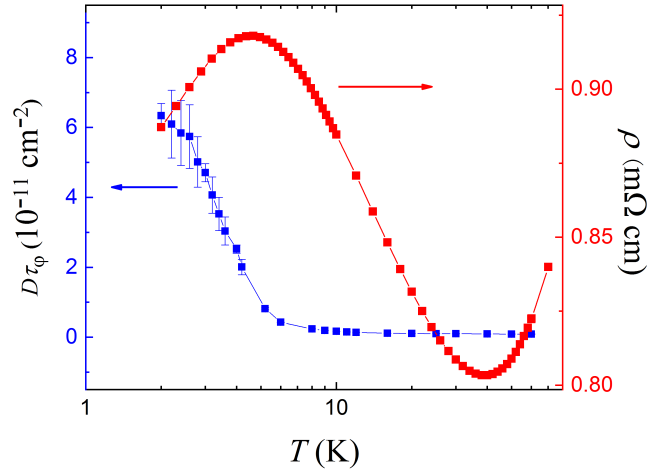
Supplementary Fig. 12| Out-of-plane MR_{\perp} of the representative $\text{Nd}_{0.88}\text{Sr}_{0.12}\text{NiO}_2$ film, fitted by HLN. MR_{\perp} ($H_{\perp\text{lab}}$) at temperatures of 8–20 K (a) and 2–4 K (b). A sign change in MR_{\perp} is seen below 7 K. (c) $\Delta\sigma/\sigma_0$ as a function of H at high temperatures. (d) $\Delta\sigma/\sigma_0$ as a function of H at low temperatures. The solid curves are fitting to the HLN Eq. (3) in the main text, by adding a H^2 term.



Supplementary Fig. 13 | Negative in-plane transverse $MR_{//}$ and out-of-plane MR_{\perp} of the representative $\text{Nd}_{0.88}\text{Sr}_{0.12}\text{NiO}_2$ film, fitted by the Kondo model. $MR_{//}$ ($H // ab, H \perp I$) at temperatures of 8–20 K (a) and MR_{\perp} ($H \perp ab$) at temperatures of 8–16 K (b). The solid curves are fitting to the Kondo model.



Supplementary Fig. 14 | Positive in-plane transverse MR_{\perp} and longitudinal MR'_{\parallel} of the representative $\text{Nd}_{0.88}\text{Sr}_{0.12}\text{NiO}_2$ film, fitted by Kondo + HLN. $MR_{\perp}(H // ab, H \perp I)$ at temperatures of 2–6 K (a) and $MR'_{\parallel}(H // ab, H // I)$ at temperatures of 2–6 K (b). The solid curves are fitting to the Kondo + HLN.



Supplementary Fig. 15| Logarithmic temperature dependence of the phase coherence time $D \cdot \tau_\phi$ (blue) and the resistivity (red) of the representative $\text{Nd}_{0.88}\text{Sr}_{0.12}\text{NiO}_2$ film at low temperatures. It is interesting to plot the phase breaking length $l_\phi^2 = D \cdot \tau_\phi$ as a function of temperature on a logarithmic scale. It is also noteworthy that in this work the dephasing length l_ϕ extracted from the fit is about 20–80 nm, much longer than the film thickness. Therefore, the phase coherent transport is two dimensional, justifying the application of the HLN equation for the data analysis. Taking $m^* \sim 20m_e$ according to the measurements of nickelate bulks [54], the calculated D is about $\sim 10^{-4} \text{ m}^2/\text{s}$, and thus estimated τ_ϕ is in the order of $\sim 10^{-11} \text{ s}$, which is consistent with that of dilute Kondo system [41]. The phase coherence time τ_ϕ shows a similar logarithmic temperature dependence as the resistivity, but the temperature range is slightly lower than that of the resistivity, the same behavior was also observed in the dilute Kondo system [55].

Supplementary Note 1: $\ln T$ -type conductance correction by weak-localization/weak-antilocalization effect and electron-electron interaction

In two-dimensional system, the quantum interference correction on conductivity in a spin-orbital coupling system gives [34]:

$$\Delta\sigma_{WL/WAL} = \alpha p \frac{e^2}{\pi h} \ln \frac{T}{T_0}. \quad (\text{SN1})$$

Here, T_0 denotes the cut-off energy, p is the dephasing exponent $\tau_\phi^{-1} \sim T^p$, and α is an effective coefficient originating from the competition of weak-localization (WL) and weak-antilocalization (WAL) effect, with $\alpha > 0$ representing the WL correction and $\alpha < 0$ representing the WAL correction. Moreover, the combination effect of electron-electron interaction (EEI) and impurity scattering can further influence the density of states and induce additional conductivity correction [34]:

$$\Delta\sigma_{EEI} = \frac{e^2}{\pi h} \left(1 - \frac{3}{4} \tilde{F}\right) \ln \frac{T}{T_1}. \quad (\text{SN2})$$

Here, $T_1 = \frac{\hbar}{k_B \tau_0}$ denotes the thermal energy scale corresponding to impurity scattering with τ_0 representing the mean free time, \tilde{F} is commonly a positive constant determined by microscopic mechanisms. Thus, the total contribution from WL/WAL and EEI corrections reads:

$$\Delta\sigma_{EEI+WL/WAL} = \left(1 + \alpha p - \frac{3}{4} \tilde{F}\right) \frac{e^2}{\pi h} \ln \frac{T}{T_0}. \quad (\text{SN3})$$

As shown in Fig. 2c in the main text, $\alpha p \approx 0.213$, thus the total value $1 + \alpha p - \frac{3}{4} \tilde{F}$ is much smaller than the value $\beta = 6.96$. To summarize, in temperature range of 8-24 K with $\ln T$ resistivity behavior, although the WL/WAL and EEI effect also contribute to the $\ln T$ resistivity, the contribution from the Kondo scattering is dominant.

Supplementary Note 2: Temperature dependence of resistivity

In the main text, we use the Hamann model to fit the measured $\rho(T)$ curves for two reasons: 1) due to the onset of superconductivity, we cannot fit the saturation of resistivity below 7 K; and 2) the Hamann model can provide more useful information, such as magnetic impurity concentration. Three underdoped $\text{Nd}_{1-x}\text{Sr}_x\text{NiO}_2$ samples ($x = 0, 0.05, 0.09$). The main results are two-fold. Firstly, all three underdoped samples are well consistent with the Kondo scattering scenario down to 0.04 K. The Hamann fitting (Supplementary Fig. 5) provide quantitative justification for this point. Moreover, all the underdoped samples demonstrate clear feature of Kondo scattering in temperature regime above T_K . Secondly, the magnetic field truly influence the R - T curves of underdoped samples with pronounced negative magnetoresistance (Supplementary Fig. 5), reminiscent of the well-known negative magnetoresistance in Kondo system (La, Ce)Al₂ [31]. Under magnetic field, the magnetoresistance can be obtained by the modified Hamman model [31] by:

$$\rho_K(T/T_K) = \rho_0 \left\{ 1 - \frac{\ln(T/T_K)}{[\ln^2(T/T_K) + s(s+1)\pi^2]^{-1/2}} \right\} \cdot \left[1 - F^2 \left(\frac{g\mu_B H}{k_B(T+T_K)} \right) \right]. \quad (\text{SN4})$$

Here, $F(x)$ is the Brillouin function for spin s and g denotes the Landé g -factor. Theoretical fitting for the R - T curves under magnetic field (as shown in Supplementary Fig. 5) by the modified Hamman mode also provide quantitative verifications for the Kondo scenario. Moreover, all three underdoped samples demonstrate the Fermi liquid behavior at low temperature below T_K .

Supplementary Note 3: Magnetoresistance fitted by Kondo model

In this work, we used the HLN model to fit the measured magnetoresistance (MR) curves, mainly because the HLN model can provide more useful information, such as the dephasing field H_ϕ and the fitting parameter α . To compare the MR with the theory, we can also use the zero temperature Kondo MR expression of Lee et. al. [56]. At zero temperature, a Kondo impurity magnetization is given as [56-58]:

$$M(H/H_1) = \begin{cases} \frac{1}{\sqrt{2\pi}} \sum_{k=0}^{\infty} \left(-\frac{1}{2}\right)^k (k!)^{-1} \left(k + \frac{1}{2}\right)^{\left(k-\frac{1}{2}\right)} e^{-(k+\frac{1}{2})} \left(\frac{H}{H_1}\right)^{2k+1}, & H \leq \sqrt{2}H_1 \\ 1 - \pi^{-\frac{3}{2}} \int \frac{dt}{t} \sin(\pi t) e^{-t \cdot \ln\left(\frac{t}{2e}\right)} \left(\frac{H}{H_1}\right) \Gamma\left(t + \frac{1}{2}\right), & \sqrt{2}H_1 \leq H \end{cases} \quad (\text{SN5})$$

where H_1 is a magnetic field scale, related to both Kondo temperature and the g-factor of impurity spin. We chose $H_1 = 11.0$ T, according to the isomagnetism $\rho(T)$ observation (see Fig. 1c). After calculating the magnetization of impurity, the zero temperature Kondo-magnetoresistance is given by:

$$R_K\left(\frac{H}{H_1}\right) = R_K(H=0) \cos^2\left(\frac{\pi}{2} M\left(\frac{H}{H_1}\right)\right). \quad (\text{SN6})$$

And the MR is given by

$$R(H) = R_0 + R_K\left(\frac{H}{H_1}\right). \quad (\text{SN7})$$

In Supplementary Fig. 13, the solid lines are the fits with the experimental negative MR data in a temperature range of 10–20 K by Eqs. SN5, SN6 and SN7. The excellent fit between experimental data and theory points towards Kondo type scattering in this temperature range.

At $T < 7$ K, the positive MR appears to be the contribution of the weak anti-localization (WAL) and/or the onset of superconductivity. Thus, we add the WAL term by using HLN equation to the Kondo interaction term in MR equation and it follows as:

$$R(H) = R_0 + R_K\left(\frac{H}{H_1}\right) - \frac{\alpha e^2}{\pi h} R_0^2 \left[\Psi\left(\frac{1}{2} + \frac{H_\phi}{H}\right) - \ln\left(\frac{H_\phi}{H}\right) \right]. \quad (\text{SN8})$$

In Supplementary Fig. 14, the solid lines are the fitting curves considering both Kondo scattering and HLN formula with the experimental positive MR data in a temperature range of 2–6K by Eq. SN8. The deviation at low temperatures and higher magnetic fields is possibly due to the onset of superconductivity. The quality of the fit strongly suggests that the WAL effect or superconductivity overrides the Kondo scattering at $T < 7$ K.

Additional references:

- [48] J. Y. Yang, W. S. Li, H. Li, Y. Sun, R. F. Dou, C. M. Xiong, L. He, and J. C. Nie, Grain size dependence of electrical and optical properties in Nb-doped anatase TiO_2 , *Appl. Phys. Lett.* 95, 213105 (2009).
- [49] D. Kaneko, K. Yamagishi, A. Tsukada, T. Manabe, and M. Naito, Synthesis of infinite-layer LaNiO_2 films by metal organic decomposition, *Physica C: Superconductivity* 469, 936-939 (2009).
- [50] M. Kawai, S. Inoue, M. Mizumaki, N. Kawamura, N. Ichikawa, and Y. Shimakawa, Reversible changes of epitaxial thin films from perovskite LaNiO_3 to infinite-layer structure LaNiO_2 , *Appl. Phys. Lett.* 94, 082102 (2009).
- [51] B. S. Liu, and C.T. Au, Carbon deposition and catalyst stability over $\text{La}_2\text{NiO}_4/\gamma\text{-Al}_2\text{O}_3$ during CO_2 reforming of methane to syngas, *Appl. Catal. A: Gen.* 244, 181-195 (2003).
- [52] M. Ferkhi, M. Rekaika, A. Khaled, M. Cassirc, and J.-J. Pireaux, Neodymium nickelate $\text{Nd}_{2-x}\text{Sr}_x\text{Ni}_{1-y}\text{Co}_y\text{O}_{4\pm d}$ (x and $y = 0$ or 0.05) as cathode materials for the oxygen reduction reaction, *Electrochimica Acta* 229, 281-290 (2017).
- [53] J. Liao, Y. Ou, H. Liu, K. He, X. Ma, Q.-K. Xue and Y. Li, Enhanced electron dephasing in three-dimensional

- topological insulators, Nat. Commun. 8, 16071 (2017).
- [54] G. Wu, J. J. Neumeier, and M. F. Hundley, Magnetic susceptibility, heat capacity, and pressure dependence of the electrical resistivity of $\text{La}_3\text{Ni}_2\text{O}_7$ and $\text{La}_4\text{Ni}_3\text{O}_{10}$, Phys. Rev. B 63, 245120 (2001).
- [55] Félicien Schopfer, Christopher Bäuerle, Wilfried Rabaud, and Laurent Saminadayar, Anomalous Temperature Dependence of the Dephasing Time in Mesoscopic Kondo Wires, Phys. Rev. Lett. 90, 056801 (2003).
- [56] M. Lee, J. R. Williams, S. Zhang, C. Daniel Frisbie, and D. Goldhaber-Gordon, Electrolyte Gate-Controlled Kondo Effect in SrTiO_3 , Phys. Rev. Lett. 107, 256601 (2011).
- [57] S. Das, A. Rastogi, L. Wu, J.-C. Zheng, Z. Hossain, Y. Zhu, and R. C. Budhani, Kondo scattering in δ -doped $\text{LaTiO}_3/\text{SrTiO}_3$ interfaces: Renormalization by spin-orbit interactions, Phys. Rev. B 90, 081107(R) (2014).
- [58] N. Andrei, K. Furuya, and J. H. Lowenstein, Solution of the Kondo problem, Rev. Mod. Phys. 55, 331-401 (1983).